Chemical Physics 140 (1990) 75–97
North-Holland

FLUORESCENCE SPECTROSCOPIC ANALYSIS OF N AND P ISOMERS OF DODCI

W. BÄUMLER and A. PENZKOFER
Naturwissenschaftliche Fakultät II – Physik, Universität Regensburg, D-8400 Regensburg, FRG

Received 20 April 1989; in final form 12 September 1989

The photoisomerization dynamics of DODCI (3,3'-diethyloxadicarbocyanine iodide) is analyzed by linear absorption and fluorescence spectroscopic measurements over a wide temperature range. The fluorescence quantum distributions and the fluorescence quantum efficiencies are measured for three excitation wavelengths. The N-isomer and P-isomer contributions to the fluorescence signals are separated. The absorption and stimulated emission cross sections of the N- and P-isomers are determined. The results are discussed by application of an angular configuration coordinate system.

1. Introduction

The photoisomerization of the polymethine dye DODCI (3,3'-diethyloxadicarbocyanine iodide) has been studied extensively by absorption and emission spectroscopy in the past. The excitation light sources used have been μs flash-lamps [1], μs pulsed dye lasers [1–7], ns *Q*-switched lasers [8–10], μs trains of pulsed mode-locked picosecond lasers [2,3,11–13], single picosecond pulses [12–22], cw mode-locked lasers [23–27], and cw dye lasers [28,29]. There is experimental evidence from rotational diffusion measurements that in the S_0 ground state DODCI molecules are in a coiled-up cis–cis conformation (normal isomer N) and the photo-excited isomer (P isomer) is in an elongated all-trans conformation [13]. Our results do not depend on the special conformation of the N isomer and P isomer. The P isomer is populated only weakly by thermal excitation [30]. The optical excitation to the S_1 state enhances the rate of molecular conformation change.

The dynamics of the conformational changes of excited DODCI molecules has been studied extensively [1–14, 17–21, 24–28, 31–34]. A three-valley S_1 potential energy surface with a low-lying minimum at a perpendicular twisting angle and a two-valley S_0 potential energy surface with high-lying barrier at a twisting angle of 90° is often used [8,9,34]. This potential energy diagram is sketched in fig. 1a. It was first applied to the photoisomerization of stilbene [35]. A four-level diagram with interisomer relaxation (fig. 1b) has been applied for a rate equation

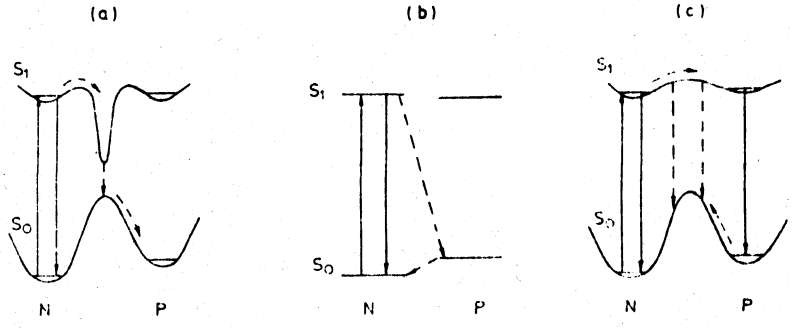

Fig. 1. Energy level models of DODCI. (a) S_1 three-valley and S_0 two-valley potential energy surfaces. (b) Four-level system. (c) S_1 and S_0 two-valley potential energy surfaces. Solid arrows, radiative absorption and emission processes. Broken arrows, nonradiative transitions.

0301-0104/90/$ 03.50 © Elsevier Science Publishers B.V.
(North Holland)

approach to the photoisomerization dynamics [7,28,29,32,33,36]. This model is very general but does not show potential energy surfaces. An S_0 and S_1 two-valley potential energy surface model (fig. 1c) sometimes has been applied successfully to polymethine dyes (bisdimethylaminoheptamethine perchlorate (BMC), pinacyanol and pseudo-isocyanine) [37].

The dye DODCI is used widely as saturable absorber for passive mode-locking of pulsed picosecond [2,3,11,15,16,38–42], cw picosecond [43–49] and cw femtosecond [46,50–58] dye lasers in the spectral region between 590 and 633 nm [11,52,56,58]. The photoisomerization influences the mode-locking behaviour of the dye [11,54,57,59,60]. DODCI has also been used as a laser dye [8,61–66]. Lasing was achieved for the P isomer [8,61–65] and the N isomer [66].

In this paper the photoisomerization dynamics of DODCI is studied by linear absorption spectroscopic [30] and fluorescence spectroscopic measurements. The dye is dissolved in methanol (CH_3OH), and ethylene glycol ($HOCH_2$–CH_2OH). Absorption spectroscopic measurements over a wide temperature range have been applied previously to determine the potential energy difference between the P and N isomer in the S_0 ground state and to determine the ground-state N and P level populations [30]. Here we concentrate on conventional fluorescence spectroscopic measurements (fluorescence quantum distribution, $E(\lambda)$, and fluorescence quantum efficiency, q) over a wide temperature range and at different excitation wavelengths to gain information on the potential energy difference between the N and P isomers in the S_1 state and on the S_1 activation energies for N→P and P→N isomerization. The N- and P-isomer fluorescence quantum distributions and fluorescence quantum efficiencies are separated. The S_1–S_0 stimulated emission cross-section spectra of the N and P photoisomers are determined separately. The experimental results are discussed by application of a three-valley S_1 potential energy surface model.

The N-isomer and P-isomer absorption and emission cross-section spectra as well as the fluorescence quantum yields are needed for a quantitative analysis of the passive mode-locking characteristics of DODCI in dye lasers.

2. Experimental

The absorption spectra of DODCI in methanol and ethylene glycol are measured at different temperatures with a conventional spectrophotometer (Beckman ACTA MIV). The S_0–S_1 long-wavelength absorption changes versus temperature are analyzed to separate the N-isomer and P-isomer absorption cross-section spectra [30].

The fluorescence spectra are measured with a self-assembled spectrofluorimeter using the front-face collection technique [67]. The arrangement is shown in fig. 2. Dye cells of 1 mm thickness are used. The dye concentrations vary with excitation wavelength, but are kept below 1.2×10^{-4} mol/dm^3 in all experiments. Up to this concentration no dimerization effects have been observed (absorption cross-section spectra, fluorescence quantum distributions, and fluorescence quantum efficiencies are independent of concentration). The dye solutions rhodamine 6G in methanol (quantum efficiency $q_R \approx 0.94$ [68–71]), rhodamine 101 in ethanol ($q_R \approx 0.98$ [71–74]), and cresyl violet in ethanol ($q_R \approx 0.56$ [75–77]) serve as reference standards for the excitation wavelength regions around 510, 590 and 625 nm, respectively. Own comparative fluorescence quantum efficiency measurements (accuracy ±2%) are in agreement with the cited fluorescence quantum efficiencies of the fluorescence standards.

The evaluation of the fluorescence quantum distribution, $E(\lambda)$, and the fluorescence quantum efficiency, q, from the detected fluorescence signal is described in appendix A. Re-absorption and re-emission

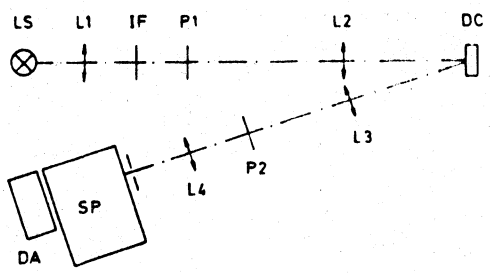

Fig. 2. Fluorescence spectroscopic setup. LS, halogen-tungsten projector lamp (Osram HLX64655, 24 V, 250 W). L1–L4, lenses. IF, interference filter. P1, P2, dichroic polarizers. DC, dye cell. SP, spectrometer. DA, diode-array system (Tracor DARRS).

of fluorescence light is included in the analysis.

For the low-temperature measurements the dye cells are inserted in a home-made optical cryostat. Suitable amounts of liquid nitrogen are applied for cooling down to −100 °C. For measuring at elevated temperatures the dye cells are put into a heating chamber with glass windows. Heat cartridges are used for heating up to 100 °C. The temperature is measured with Pt 100 resistors.

3. Results

The absorption spectra of DODCI in methanol and ethylene glycol are determined at three temperatures and the N-isomer and P-isomer absorption cross-section spectra are separated [30].

The fluorescence quantum distribution spectra, $E(\lambda)$, and the fluorescence quantum efficiencies, q, are measured for three excitation wavelengths at various temperatures. The N-isomer and P-isomer fluorescence contributions are separated and interpreted.

3.1. Absorption spectra

The apparent absorption cross-section spectra [78] of DODCI in methanol at −80 °C, 21.5 °C and 60 °C are shown in fig. 3. For DODCI in ethylene glycol the apparent absorption spectra at 2 °C, 21.5 °C and 95 °C are plotted in fig. 4. $\sigma'(\lambda)=\alpha(\lambda)/N_0$ is displayed in the graphs, where α is the absorption coefficient and N_0 is the total number density of DODCI molecules (N isomers and P isomers together). The long-wavelength spectral changes with temperature indicate the thermal population of the P isomer in the electronic S_0 ground state.

The N-isomer absorption cross-section spectra $\sigma_N(\lambda)=\alpha_N(\lambda)/N_N$ and the P-isomer absorption cross-section spectra $\sigma_P(\lambda)=\alpha_P(\lambda)/N_P$ are separated in figs. 5 and 6 following the procedure described in ref. [30] ($\alpha=\alpha_N+\alpha_P$): First the energy difference E_P^0 between the S_0 ground-state levels of the P isomer and the N isomer is determined by temperature-dependent absorption measurements [30]. The E_P^0 values are listed in table 1. The mole fraction $x_{P,th}^0$ of P isomers in the S_0 ground state at thermal equilibrium is

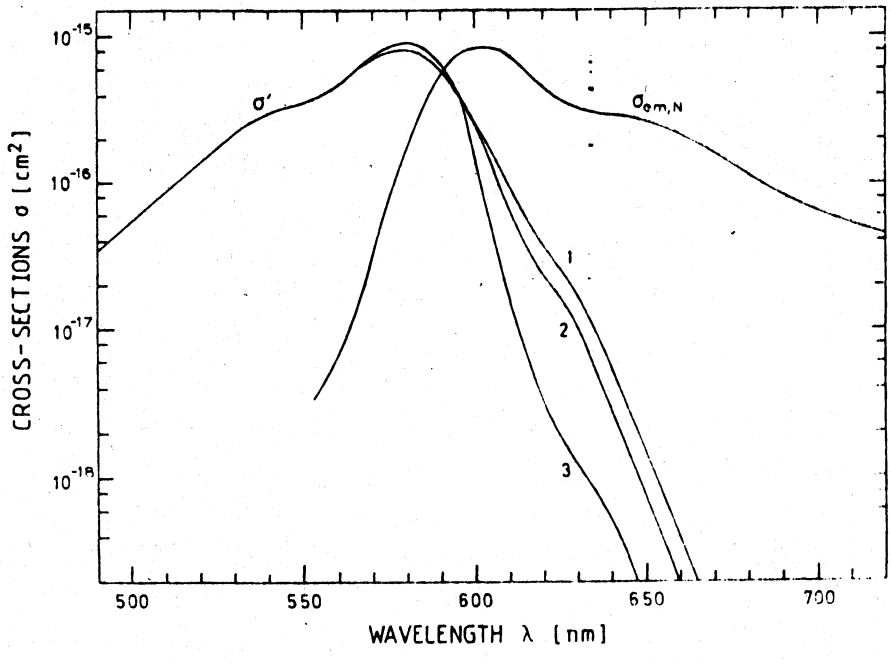

Fig. 3. Apparent absorption cross-section spectra, $\sigma'(\lambda)$, of DODCI in methanol at (1) $\vartheta=60$ °C, (2) $\vartheta=21.5$ °C, and (3) $\vartheta=-80$ °C. The stimulated emission cross-section spectrum of the N isomer, $\sigma_{em,N}$, is included ($\lambda_f=590$ nm, $\vartheta=0$ °C).

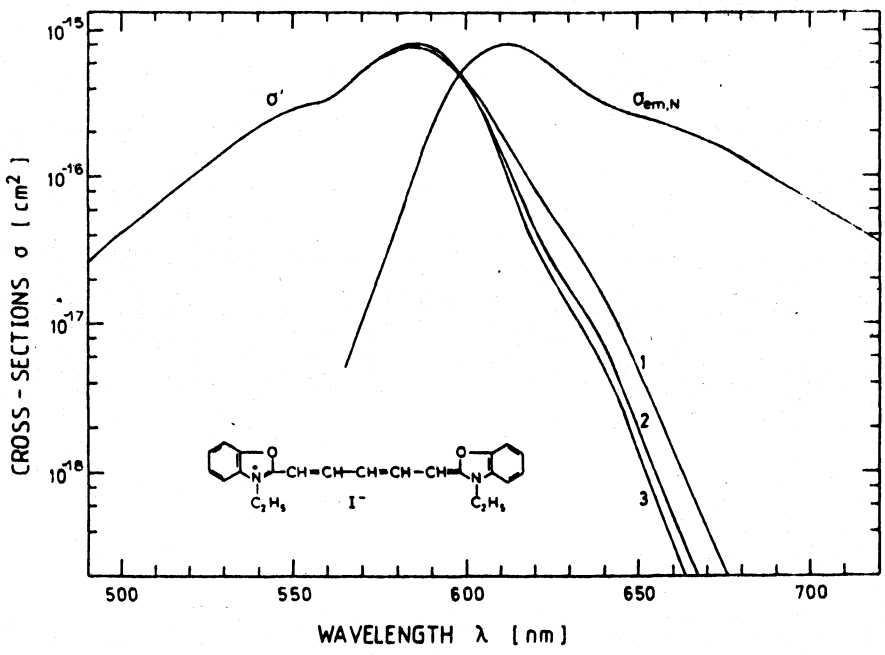

Fig. 4. Apparent absorption cross-section spectra. $\sigma'(\lambda)$, of DODCI in ethylene glycol at (1) $\vartheta = 95°C$, (2) $\vartheta = 21.5°C$, and (3) $\vartheta = 2°C$. Also the stimulated emission cross-section spectrum of the N isomer, $\sigma_{em,N}$, is shown ($\lambda_L = 597$ nm, $\vartheta = 22°C$). The structural formula of DODCI is included.

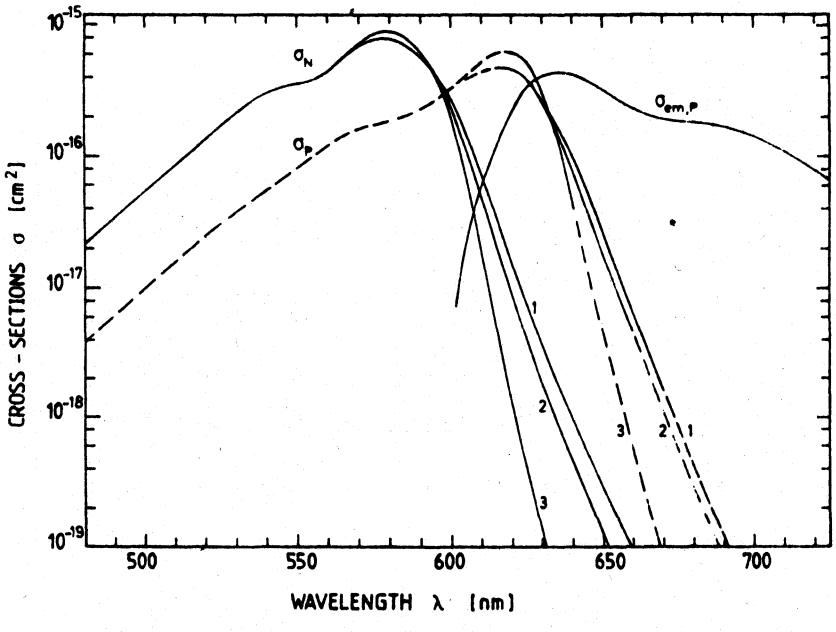

Fig. 5. Separated absorption and emission cross-section spectra of DODCI in methanol. σ_N, N-isomer absorption cross-section spectra and σ_P, P-isomer cross-section spectra at (1) $\vartheta = 60°C$, (2) $\vartheta = 21.5°C$, and (3) $\vartheta = -80°C$. $\sigma_{em,P}$, stimulated emission cross-section spectrum of P isomer ($\vartheta = 22°C$).

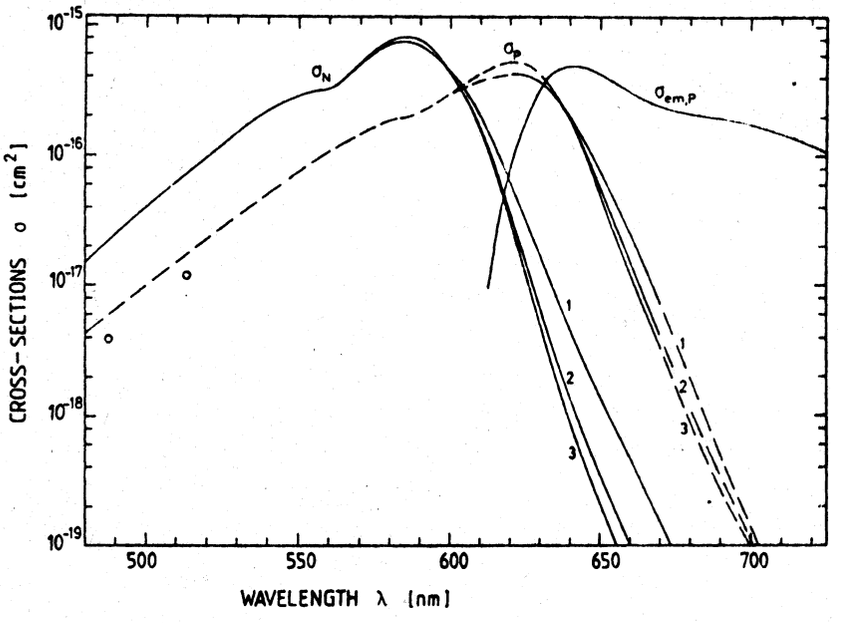

Fig. 6. Separated absorption and emission cross-section spectra of DODCI in ethylene glycol. σ_N, N-isomer absorption cross-section spectra and σ_P, P-isomer absorption cross-section spectra at (1) $\vartheta = 95$°C, (2) $\vartheta = 21.5$°C, and (3) $\vartheta = 2$ °C. $\sigma_{em,P}$, stimulated emission cross-section spectrum of P isomer ($\vartheta = 22$°C).

Table 1
Spectroscopic data of DODCI in methanol and ethylene glycol. Most parameters are explained in figs. 19 and 20

Solvent	Methanol	Ethylene glycol	Comments
$\tau_{rad,N}$ (ns)	2.45	2.35	eq. (11)
$\tau_{rad,P}$ (ns)	≈5.1	≈4.1	eq. (11)
$\int\sigma_{abs,N}(\tilde{\nu})d\tilde{\nu}$ (cm)	1.35×10^{-12}	1.25×10^{-12}	
$\int\sigma_{abs,P}(\tilde{\nu})d\tilde{\nu}$ (cm)	$\approx7.3\times10^{-13}$	$\approx8\times10^{-13}$	
$\int\sigma_{em,N}(\tilde{\nu})d\tilde{\nu}$ (cm)	1.19×10^{-12}	1.09×10^{-12}	eq. (12)
$\int\sigma_{em,P}(\tilde{\nu})d\tilde{\nu}$ (cm)	$\approx6.4\times10^{-13}$	$\approx7\times10^{-13}$	eq. (12)
E_η (cm^{-1})	928	2171	ref. [95]
E_P^0 (cm^{-1})	703 ± 50	727 ± 50	this work and ref. [30]
$x_{P,th}^0$ (25°C)	0.0325	0.029	this work and ref. [30]
E_N^{01} (cm^{-1})	16920 ± 50	16710 ± 50	eq. (21)
E_P^{01} (cm^{-1})	15950 ± 50	15840 ± 50	eq. (22)
E_P^1 (cm^{-1})	270 ± 100	143 ± 100	eq. (23)
E_A^0 (cm^{-1})	5005	≈5005	ref. [8]
E_A^0 (cm^{-1})	4077	-	$E_A^0 - E_\eta$
$E_{A,N}^1$ (cm^{-1})	2380 ± 150	2650 ± 200	eq. (20) and fig. 21
$E_{A,N}^1$ (cm^{-1})	1450 ± 150	-	$E_{A,N}^1 - E_\eta$
$E_{A,P}^1$ (cm^{-1})	2680 ± 50	2470 ± 60	eq. (20) and fig. 21
$E_{A,P}^1$ (cm^{-1})	1750 ± 50	-	$E_{A,P}^1 - E_\eta$
$\Delta E_{N,P}^1$ (cm^{-1})	−33 ± 300	323 ± 360	eq. (25)

$$x^0_{P,th} = \frac{N_{P,S_0}}{N_{N,S_0}+N_{P,S_0}} = \frac{\exp(-E^0_P/k_B\vartheta)}{1+\exp(-E^0_P/k_B\vartheta)}. \quad (1)$$

N_{P,S_0} is the number density of P isomers in the S_0 state and N_{N,S_0} is the number density of N isomers in the S_0 state. ϑ is the temperature. The mole fraction of N isomers in the ground state at thermal equilibrium is $x^0_{N,th} = 1 - x^0_{P,th}$.

At the short-wavelength side ($\lambda < \lambda_{0,N}$, $\lambda_{0,N}$ is the zero-vibration electronic S_0–S_1 transition wavelength of the N isomer) σ_N is separated from σ' by $\sigma_N \approx \sigma'/x^0_{N,th}$. At the long-wavelength side ($\lambda > \lambda_{0,N}$) σ_N is determined approximately by [78]

$$\sigma_N(\lambda) \approx \sigma_{N,em}(\lambda) \exp\left[-\frac{hc_0}{k_B\vartheta}\left(\frac{1}{\lambda_{0,N}}-\frac{1}{\lambda}\right)\right]. \quad (2)$$

$\sigma_{N,em}(\lambda)$ is the stimulated emission cross-section spectrum of the N isomer. h is the Planck constant, c_0 is the velocity of light in vacuum, and k_B is the Boltzmann constant. The exponential factor gives the fraction of molecules taking part in the absorption at the long-wavelength side.

The absorption cross-section spectrum of the ground-state P isomers is determined by $\sigma' = x^0_{N,th}\sigma_N + x^0_{P,th}\sigma_P$ leading to

$$\sigma_P(\lambda) = \frac{\sigma' - (1-x^0_{P,th})\sigma_N}{x^0_{P,th}}. \quad (3)$$

The solid $\sigma_P(\lambda)$ curves of figs. 5 and 6 are obtained by use of eq. (3). The dashed extensions are determined by assuming the same spectral shape of the absorption cross-section spectra of the P isomer and the N isomer. For DODCI in ethylene glycol the P-isomer absorption cross sections at 488 and 514 nm have been determined separately by P-isomer ground-state accumulation studies with an argon ion laser [79]. The two experimental points (circles) agree reasonably well with the shape extensions.

The ratio of P-isomer absorption to total absorption, $\alpha_P(\lambda)/\alpha(\lambda)$, is

$$\frac{\alpha_P(\lambda)}{\alpha(\lambda)} = \frac{N_{P,S_0}\sigma_P(\lambda)}{N_{P,S_0}\sigma_P(\lambda)+N_{N,S_0}\sigma_N(\lambda)} = \frac{N_{P,S_0}\sigma_P(\lambda)}{N_0\sigma'(\lambda)} = \frac{x^0_{P,th}\sigma_P(\lambda)}{\sigma'(\lambda)}. \quad (4)$$

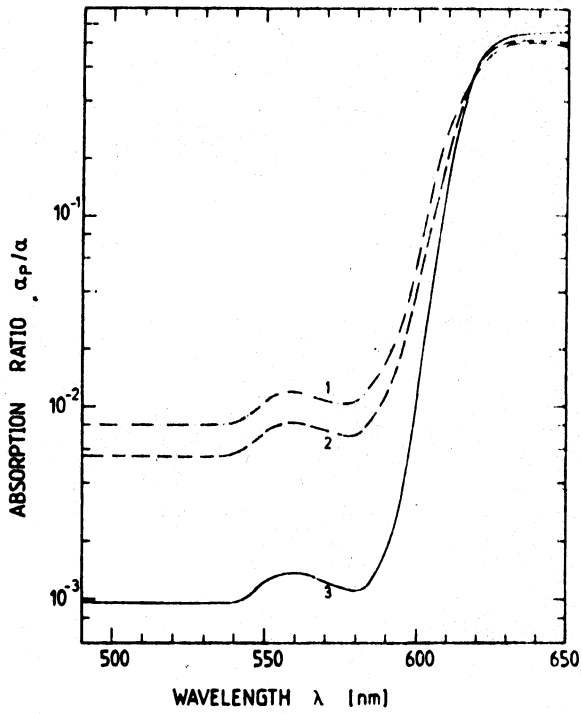

Fig. 7. Ratio of P-isomer absorption coefficient to total absorption coefficient versus excitation wavelength for DODCI in methanol. (1) $\vartheta = 60$°C, (2) $\vartheta = 21.5$°C, (3) $\vartheta = -80$°C.

N_0 is the total number density of DODCI molecules. In figs. 7 and 8 the ratios α_P/α are displayed for DODCI in methanol and ethylene glycol, respectively. Curves are shown for three different temperatures. At the short-wavelength side ($\lambda < \lambda_{0,N}$) the N-isomer absorption dominates ($x^0_{P,th}$ in the per cent region and $\sigma_P(\lambda) < \sigma_N(\lambda)$) while at the long-wavelength side the absorption of the P isomers is dominant ($\sigma_P(\lambda) \gg \sigma_N(\lambda)$).

3.2. Fluorescence studies

The fluorescence behaviour of DODCI in methanol and ethylene glycol is studied as a function of excitation wavelength and temperature. Fluorescence quantum efficiencies, q, and fluorescence quantum distributions, $E(\lambda)$, are determined. First, overall spectra are presented and then the N-isomer and P-isomer contributions are separated.

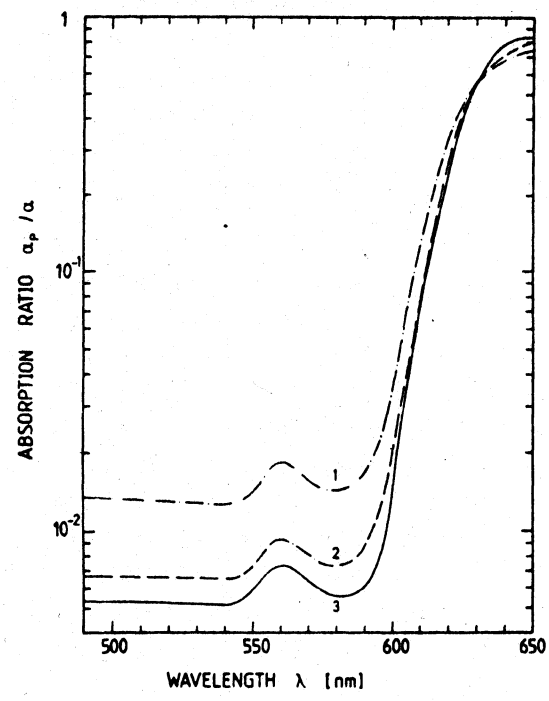

Fig. 8. Absorption ratio α_P/α of DODCI in ethylene glycol. (1) $\vartheta = 95$°C, (2) $\vartheta = 22$°C, and (3) $\vartheta = 2$°C.

3.2.1. Total fluorescence spectra

The fluorescence quantum efficiencies, q, versus temperature, are plotted in figs. 9a and 9b for three excitation wavelengths. The fluorescence quantum efficiencies rise with decreasing temperature and approach 100%. An Arrhenius-type activation energy has to be overcome for efficient fluorescence quenching (twisting of molecule to 90° out-of-plane orientation in the transfer from cis–cis to all-trans arrangement, see below [80–84]). The fluorescence quantum efficiencies for $\lambda_L = 510$ nm and $\lambda_L = \lambda_{0,N}$ are approximately equal. Only at low temperatures does $q(510\ \text{nm})$ seem to be slightly less than $q(\lambda_{0,N})$. At $\lambda_L = 624$ nm (DODCI in methanol) and $\lambda_L = 630$ nm (DODCI in ethylene glycol) the P isomer is excited preferentially (fig. 7). High fluorescence quantum efficiencies are obtained at low temperatures. At elevated temperatures the fluorescence becomes smaller than for short-excitation wavelengths (longer S_1-state radiative lifetime of P isomer, see section 3.3 below).

Some fluorescence quantum distributions, $E(\lambda)$, at different excitation wavelengths and temperatures are presented in figs. 10–12 for DODCI in methanol, and in figs. 13–15 for DODCI in ethylene glycol.

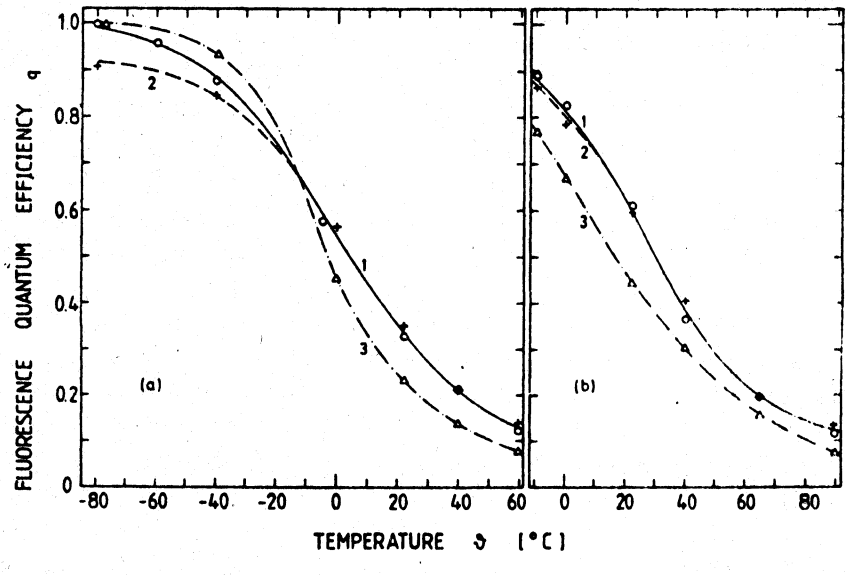

Fig. 9. Fluorescence quantum efficiencies versus temperature for three different excitation wavelengths λ_L. (a) DODCI in methanol (1, ○) $\lambda_L = 590$ nm, (2, +) $\lambda_L = 510$ nm, and (3, △) $\lambda_L = 624$ nm. (b) DODCI in ethylene glycol (1, ○) $\lambda_L = 597$ nm, (2, +) $\lambda_L = 510$ nm, and (3, △) $\lambda_L = 630$ nm.

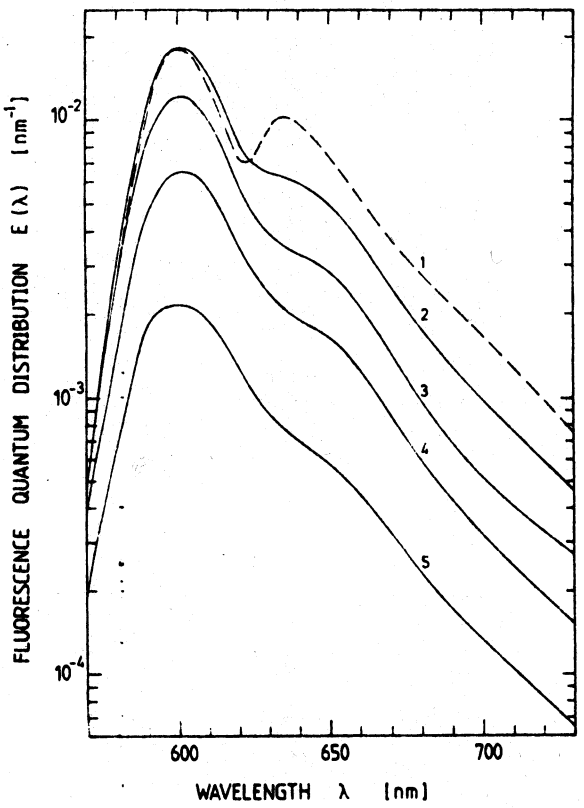

Fig. 10. Fluorescence quantum distribution of DODCI in methanol. Excitation wavelength $\lambda_L = 590$ nm (full spectral width of excitation light $\Delta\lambda_L = 9$ nm). The temperatures are $\vartheta = -80$°C (1), −40°C (2), −5°C (3), 22°C (4), and 60°C (5).

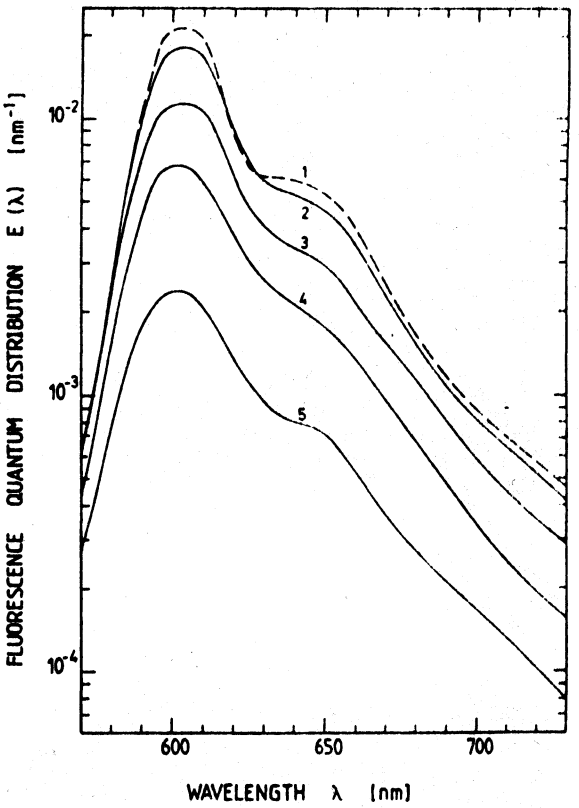

Fig. 11. Fluorescence quantum distribution of DODCI in methanol for $\lambda_L = 510$ nm ($\Delta\lambda_L = 5.2$ nm). The curves belong to $\vartheta = -80$°C (1), −40°C (2), 0°C (3), 22°C (4), and 60°C (5).

In fig. 10 the excitation wavelength is $\lambda_L = 590$ nm. It is near the zero-vibration S_0–S_1 excitation wavelength of the N isomer ($\lambda_{0,N} \approx 591$ nm, fig. 3). At $\vartheta = -80$°C additionally to the N-isomer peak around 600 nm there appears the P-isomer fluorescence peak around 635 nm. The P-isomer fluorescence peak is thought to be due to accumulation of molecules in the S_0 P-isomer ground state by the excitation light (very long P-isomer to N-isomer relaxation time in the ground state). The absorption of excitation light from the accumulated population of the P-isomer S_0 state leads to the enhanced P-isomer fluorescence. At temperatures above −40°C the population accumulation in the P-isomer S_0 state becomes negligible for the applied excitation intensities. An analysis of the accumulation dynamics is given in appendix B. Above −40°C the fluorescence quantum distribution curves broaden with rising temperature. This broadening is more clearly seen in fig. 13a where $E(\lambda)/E_{max}$ is plotted for $\vartheta = -5$°C and $\vartheta = 60$°C. Around the P-isomer fluorescence peak the rise of $E(\lambda)/E_{max}$ with temperature is thought to be partially due to thermal broadening of the fluorescence. Some contribution could be due to enhanced P-isomer fluorescence due to S_1-state N-isomer to P-isomer transfer (adiabatic S_1-state N-isomer to P-isomer transition). An estimate of the contribution of thermal broadening of the N-isomer fluorescence to the rise of $E(635\text{ nm})/E_{max}$ may be obtained by comparing the thermal rise of the absorption analog $\sigma'(530\text{ nm})/\sigma'_{max}$. For a temperature change from 22°C to 60°C the rise of the absorption ratio is approximately 1.08, while the rise of

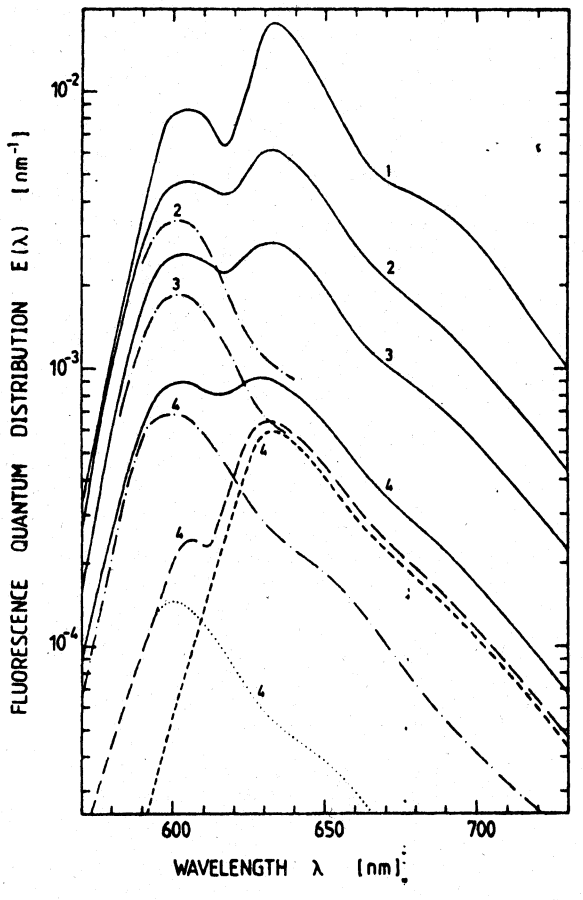

the normalized fluorescence quantum distribution is 1.15 for the same temperature interval. For another comparison, $E(585\ \text{nm})/E_{max}$ of rhodamine 6G in ethanol increases by a factor of 1.07 in heating from 22°C to 60°C.

The fluorescence spectra for $\lambda_L = 510$ nm are shown in fig. 11. Even at −80°C the ground-state P-isomer accumulation is weak and therefore no pronounced P-isomer fluorescence peak is seen. (For a discussion see appendix B.) Again with rising temperature the fluorescence around the P-isomer emission peak ($\lambda \approx 635$ nm) increases relative to the N-isomer emission peak ($\lambda \approx 602$ nm). This behaviour is more directly seen in fig. 13b where $E(\lambda)/E_{max}$ is plotted. A comparison of the dotted curve (excitation wavelength $\lambda_L = 590$ nm, $\vartheta = 0$°C) with the solid curve 1 ($\lambda_L = 510$ nm, $\vartheta = 0$°C) indicates a larger fluorescence enhancement around the P-isomer peak for short-wavelength excitation. This fluorescence be-

◀ Fig. 12. Fluorescence quantum distribution of DODCI in methanol. Excitation wavelength $\lambda_L = 624$ nm ($\Delta\lambda_L = 11$ nm). The solid curves present the total fluorescence quantum distribution $E(\lambda)$. The dash-dotted curves give the contributions $x_N^l E_N(\lambda)$. The long-dashed curve is $E(\lambda) - x_N^l E_N(\lambda)$, the short-dashed curve is $x_P^l E_P(\lambda)$, and the dotted curve is $\phi_{PN}^l x_P^l E_N(\lambda)$. (1) $\vartheta = -80$°C, (2) $\vartheta = 0$°C, (3) $\vartheta = 22$°C, (4) $\vartheta = 60$°C.

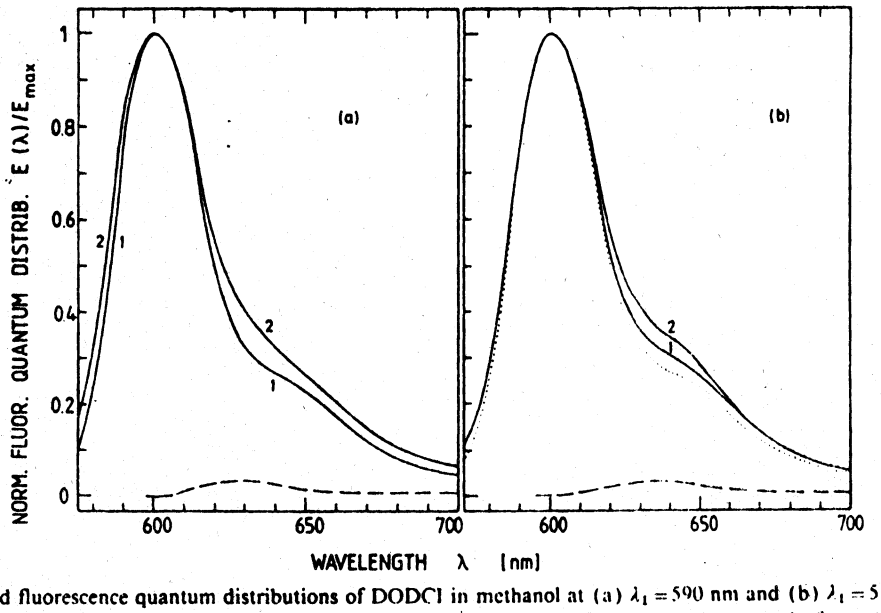

Fig. 13. Normalized fluorescence quantum distributions of DODCI in methanol at (a) $\lambda_L = 590$ nm and (b) $\lambda_L = 510$ nm. The solid curves belong to the temperatures (1) 0°C and (2) 60°C. The dotted curve in part (b) reproduces curve 1 of part (a) ($\lambda_L = 590$ nm, $\vartheta = 0$°C). The dashed curves represent $(x_P^l + \phi_{NP}^l)E_P(\lambda)$ for (a) $\lambda_L = 590$ nm, $\vartheta = 60$°C, and (b) $\lambda_L = 510$ nm, $\vartheta = 0$°C.

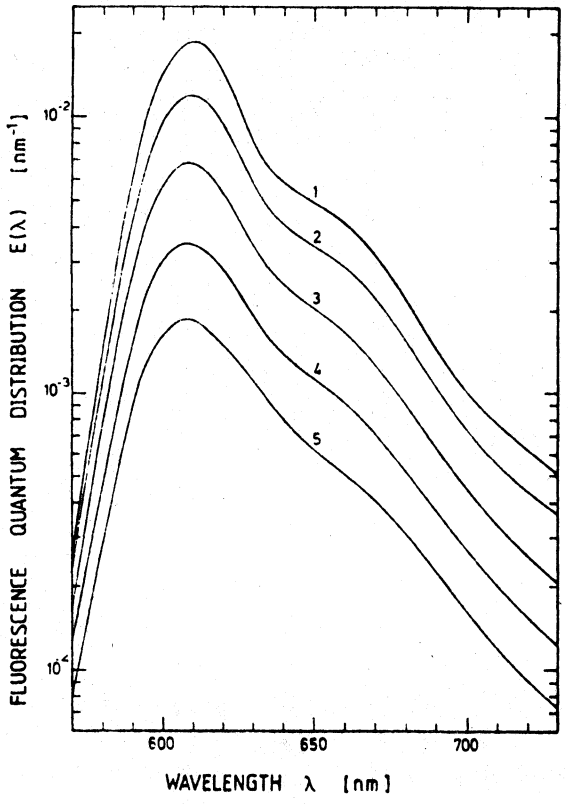

Fig. 14. Fluorescence quantum distribution of DODCI in ethylene glycol. Excitation wavelength $\lambda_L = 597$ nm ($\Delta\lambda_L = 9$ nm). The temperatures are (1) −10°C, (2) 22°C, (3) 40°C, (4) 65°C and (5) 90°C.

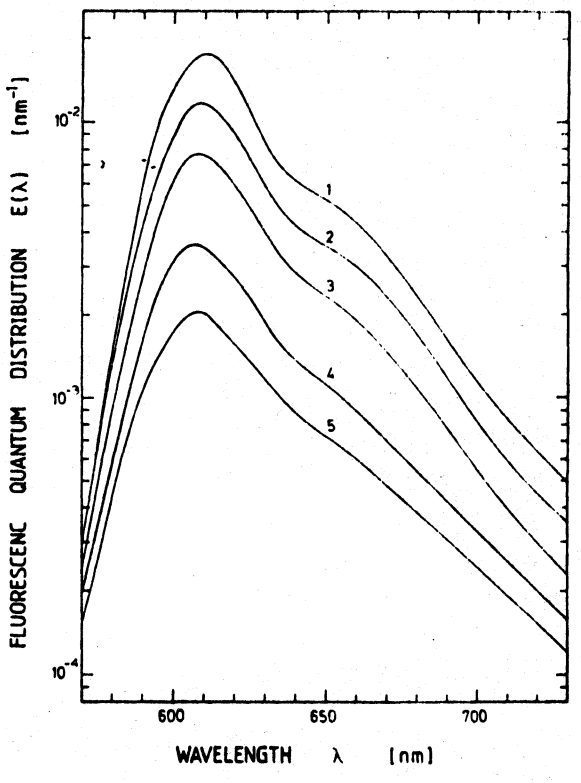

Fig. 15. Fluorescence quantum distribution of DODCI in ethylene glycol. Excitation wavelength $\lambda_L = 510$ nm ($\Delta\lambda_L = 5.2$ nm). The temperatures are (1) −10°C, (2) 22°C, (3) 40°C, (4) 65°C, and (5) 90°C.

haviour might be interpreted as an enhanced S_1-state N-isomer to P-isomer transfer rate at short-wavelength excitation. It is compatible with recent P-isomer accumulation studies on DODCI in ethylene glycol where an enhanced N-isomer to P-isomer transfer rate is obtained at short-wavelength excitation [79].

The solid curves in fig. 12 display the fluorescence quantum distribution, $E(\lambda)$, at the excitation wavelength of $\lambda_L = 624$ nm. The P-isomer fluorescence dominates. The N-isomer fluorescence gains importance with rising temperature. This behaviour may be due partly to an enhanced N-isomer absorption with rising temperature (see $\alpha_P(\lambda)/\alpha(\lambda)$ curves of fig. 7) and due to an increasing S_1-state P-isomer to N-isomer transfer rate.

The fluorescence quantum distributions of DODCI in ethylene glycol are displayed in the figs. 14–17. The fluorescence behaviour for $\lambda_L = 597$ nm (figs. 14 and 17a) and $\lambda_L = 510$ nm (figs. 15 and 17b) is very similar to the situation of DODCI in methanol. For the case of long-wavelength excitation, $\lambda_L = 630$ nm, the P-isomer fluorescence and that of the N isomer seem to be of the same strength and the P-isomer to N-isomer fluorescence ratios seem to be independent of temperature. In fig. 8 it is seen that the absorption ratio $\alpha_P(630\text{ nm})/\alpha(630\text{ nm})$ is approximately temperature independent. Laser-induced P-isomer accumulation studies [79] indicate a very weak P-isomer to N-isomer transfer rate at 630 nm.

3.2.2. Separated N-isomer and P-isomer fluorescence spectra

In the following the total fluorescence quantum efficiencies, q, and fluorescence quantum distribu-

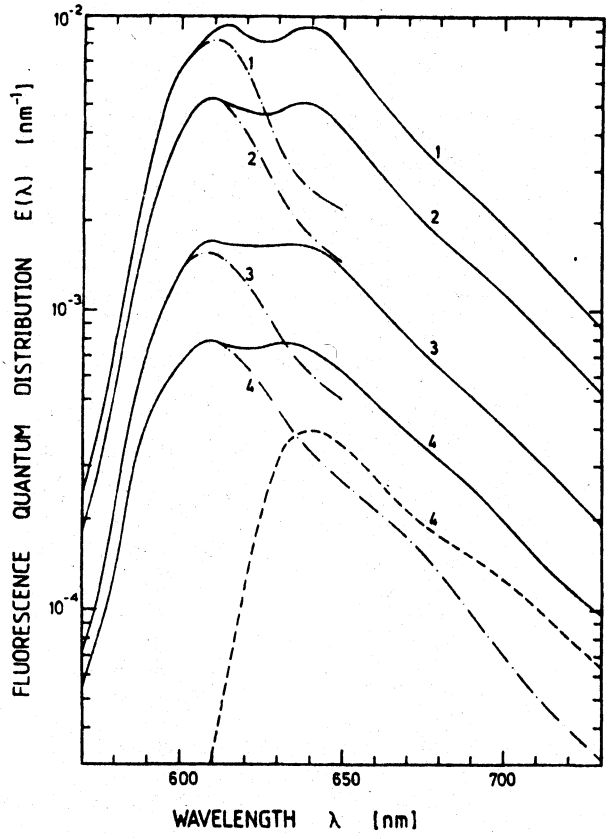

tions, $E(\lambda)$, are separated into the N-isomer and P-isomer contributions. First the separation procedure is described and then the results are presented.

3.2.2.1. Separation procedure. Referring to the S_0 and S_1 potential energy surface models (figs. 1a and 1c or figs. 19 and 20) the total fluorescence quantum efficiency, q, may be described generally by

$$q = x_N^1 q_N + x_N^1 \phi_{NP}^1 q_P + x_P^1 q_P + x_P^1 \phi_{PN}^1 q_N$$
$$= (x_N^1 + x_P^1 \phi_{PN}^1) q_N + (x_P^1 + x_N^1 \phi_{NP}^1) q_P$$
$$= q_N' + q_P' . \qquad (5)$$

$x_N^1 = \alpha_N(\lambda_L)/\alpha(\lambda_L)$ is the fraction of molecules in the S_1 state which is excited from the N-isomer S_0 ground state to the N-isomer S_1 state (fraction of excitation photons absorbed by N isomers), while

◀ Fig. 16. Fluorescence quantum distribution of DODCI in ethylene glycol at $\lambda_L = 630$ nm ($\Delta\lambda_L = 15.8$ nm). The solid curves represent the total fluorescence quantum distribution $E(\lambda)$. The dash-dotted curves give the contribution $x_N^1 E_N(\lambda)$. The short-dashed curve is $x_P^1 E_P(\lambda)$. The temperatures are (1) $\vartheta = -10$°C, (2) $\vartheta = 22$°C, (3) $\vartheta = 65$°C and (4) $\vartheta = 90$°C.

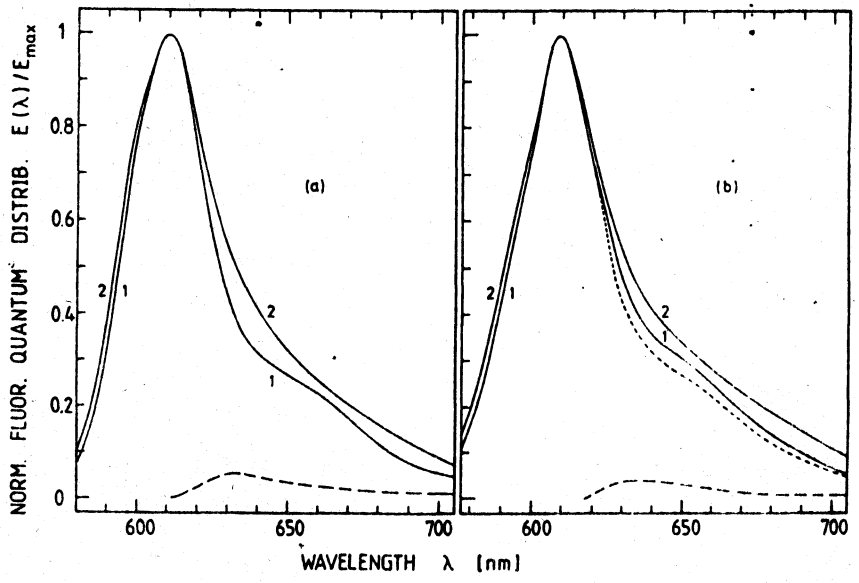

Fig. 17. Normalized fluorescence quantum distributions of DODCI in ethylene glycol at (a) $\lambda_L = 597$ nm and (b) $\lambda_L = 510$ nm. The solid curves belong to the temperatures (1) $\vartheta = -10$°C, and (2) 90°C. The short-dashed curve in part (b) reproduces curve 1 of part (a) ($\lambda_L = 597$ nm, $\vartheta = -10$°C). The dashed curves represent $(x_P^1 + \phi_{NP}^1) E_P(\lambda)$ for (a) $\lambda_L = 597$ nm, $\vartheta = 90$°C, and (b) $\lambda_L = 510$ nm, $\vartheta = -10$°C.

$x_P^1 = \alpha_P(\lambda_L)/\alpha(\lambda_L)$ is the fraction of molecules in the S_1 state which is excited from the P-isomer ground state to the P-isomer S_1 state. The relations for x_N^1 and x_P^1 are derived by the following considerations: excitation rate of N isomers

$$k_{exc}^N = \sigma_N(\lambda_L) N_{N,S_0} I_L = \alpha_N(\lambda_L) I_L ;$$

excitation rate of P isomers

$$k_{exc}^P = \sigma_P(\lambda_L) N_{P,S_0} I_L = \alpha_P(\lambda) I_L ;$$

total excitation rate

$$k_{exc} = k_{exc}^N + k_{exc}^P = [\alpha_N(\lambda_L) + \alpha_P(\lambda_L)] I_L = \alpha(\lambda_L) I_L ;$$

$$x_N^1 = k_{exc}^N / k_{exc} = \alpha_N(\lambda_L)/\alpha(\lambda_L) ;$$

$$x_P^1 = k_{exc}^P / k_{exc} = \alpha_P(\lambda_L)/\alpha(\lambda_L) ;$$

$$x_N^1 + x_P^1 = 1 .$$

$\alpha_P/\alpha = x_P^1$ versus wavelength λ is shown in figs. 7 and 8. q_N is the fluorescence quantum efficiency of the N isomers (fraction of excited N isomers that emit radiatively within the N-isomer S_1–S_0 level scheme) and q_P is the fluorescence quantum efficiency of the P isomers. ϕ_{NP}^1 gives the fraction of excited N isomers that transfer to P isomers in the S_1 band, and ϕ_{PN}^1 is the fraction of initially excited P isomers that transfer to N isomers in the S_1 band.

Analogous to the fluorescence quantum efficiency, q, the fluorescence quantum distribution, $E(\lambda)$, is given by

$$E(\lambda) = (x_N^1 + x_P^1 \phi_{PN}^1) E_N(\lambda) + (x_P^1 + x_N^1 \phi_{NP}^1) E_P(\lambda)$$
$$= E_N'(\lambda) + E_P'(\lambda) . \qquad (6)$$

Eqs. (5) and (6) may be simplified for the two experimental situations of (a) short-wavelength excitation $\lambda_L < \lambda_{0,N}$ ($\lambda_{0,N}$ is the wavelength of zero-vibration S_0–S_1 N-isomer excitation) and (b) long-wavelength excitation $\lambda_L > \lambda_{P,max}^{abs}$ ($\lambda_{P,max}^{abs}$ is the wavelength of maximum S_0–S_1 absorption cross section of P isomer).

(a) *Short-wavelength excitation ($\lambda_L \leqslant \lambda_{0,N}$).* The direct P-isomer excitation becomes small ($x_P^1 \lesssim 0.01$, see figs. 7 and 8). The term $x_P^1 \phi_{PN}^1$ may be neglected compared to x_N^1 and $x_N^1 = 1 - x_P^1$ may be replaced by 1. With these approximations, eqs. (5) and (6) reduce to

$$q(\lambda_L, \vartheta) = q_N'(\lambda_L, \vartheta) + q_P'(\lambda_L, \vartheta)$$
$$\approx q_N(\lambda_L, \vartheta) + [x_P^1 + \phi_{NP}^1(\lambda_L, \vartheta)] q_P(\lambda, \vartheta) , \qquad (7)$$

$$E(\lambda, \lambda_L, \vartheta) = E_N'(\lambda, \lambda_L, \vartheta) + E_P'(\lambda, \lambda_L, \vartheta)$$
$$\approx E_N(\lambda, \lambda_L, \vartheta)$$
$$+ [x_P^1 + \phi_{NP}^1(\lambda_L, \vartheta)] E_P(\lambda, \lambda_L, \vartheta) . \qquad (8)$$

$q_N' \approx q_N$ and $E_N'(\lambda) \approx E_N(\lambda)$ are the dominant contributions. An accurate separation of q_P' or $E_P'(\lambda)$ from q or $E(\lambda)$ is not possible. For a crude separation procedure one may assume (i)

$$E(\lambda, \lambda_{0,N}, 0°C) = E_N(\lambda, \lambda_L, 0°C)$$

and (ii)

$$E_N(\lambda, \lambda_L, \vartheta)/E_{max}(\lambda_L, \vartheta)$$
$$= \tfrac{1}{2}[E(\lambda, \lambda_L, \vartheta)/E_{max}(\lambda_L, \vartheta)$$
$$+ E_N(\lambda, \lambda_L, 0°C)/E_{max}(\lambda_L, 0°C)] .$$

The first approximation (i) overestimates $E_N(\lambda, \lambda_L, 0°C)$ somewhat since the P-isomer contribution to $E(\lambda, \lambda_{0,N}, 0°C)$ is neglected. For the second approximation (ii) it is assumed that the rise of the fluorescence quantum distribution around the P-isomer fluorescence peak, $\lambda_{P,max}$, is due in equal parts to the thermal broadening of the N-isomer fluorescence and to the S_1-state transfer of N isomers to P isomers.

(b) *Long-wavelength excitation ($\lambda_L \geqslant \lambda_{P,max}^{abs}$).* The P-isomer absorption becomes larger than the N-isomer absorption (figs. 7 and 8). The N-isomer to P-isomer S_1-state transfer term $x_N \phi_{NP}^1 q_P$ (eq. (5)) may be neglected and eqs. (5) and (6) reduce to

$$q(\vartheta) \approx x_N^1 q_N + x_P^1 \phi_{PN}^1 q_N + x_P^1 q_P , \qquad (9)$$

$$E(\lambda, \vartheta) \approx x_N^1 E_N(\lambda, \vartheta) + x_P^1 \phi_{PN}^1 E_N(\lambda, \vartheta)$$
$$+ x_P^1 E_P(\lambda, \vartheta) . \qquad (10)$$

$E_N(\lambda, \vartheta)$ is set equal to $E_N(\lambda, \lambda_{0,N}, \vartheta)$ which is nearly equal to $E(\lambda, \lambda_{0,N}, \vartheta)$. $x_N^1(\lambda_L, \vartheta) = 1 - x_P^1(\lambda_L, \vartheta)$ is taken from figs. 7 and 8. $x_N^1 E_N(\lambda, \vartheta)$ is separated from $E(\lambda, \vartheta)$. The remaining part is entangled in $x_P^1 E_P(\lambda, \vartheta)$ and $x_P^1 \phi_{PN}^1 E_N(\lambda, \vartheta)$ by trial and error avoiding a break in the $x_P^1 E_P(\lambda, \vartheta)$ curve around $\lambda_{N,max}^{em}$, the peak N-isomer emission wavelength.

3.2.2.2. Separation results.

(a) *Long-wavelength excitation.* For DODCI in methanol the separation of $E(\lambda)$ at $\vartheta = 60°C$

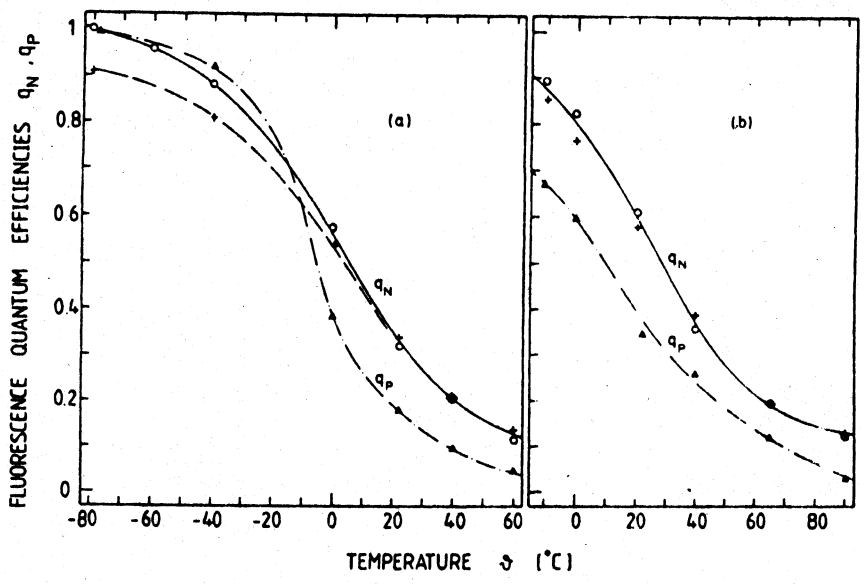

Fig. 18. Fluorescence quantum efficiencies of N isomer, q_N, and P isomer, q_P, versus temperature for (a) DODCI in methanol and (b) DODCI in ethylene glycol. (+) q_N belonging to $\lambda_L = 510$ nm, (○) q_N belonging to $\lambda_L \approx \lambda_{0,N}$, (△) q_P values.

into $x_N^l E_N(\lambda)$ (dash-dotted curve 4) and $x_P^l \phi_{PN}^l E_N(\lambda) + x_P^l E_P(\lambda)$ (long-dashed curve) as well as the entanglement of $x_P^l \phi_{PN}^l E_N(\lambda) + x_P^l E_P(\lambda)$ into $x_P^l \phi_{PN}^l E_N(\lambda)$ (dotted curve) and $x_P^l E_P(\lambda)$ (short-dashed curve) is shown in fig. 12. $E_P(\lambda)$ is obtained from $x_P^l E_P(\lambda)$ since x_P^l is known (fig. 7). $q_P = \int E_P(\lambda)\, d\lambda$ of DODCI in methanol is plotted in fig. 18a versus temperature. From the dotted curve in fig. 12 a value of $\phi_{PN}^l(60°C) \approx 0.09$ is extracted ($x_P^l \phi_{NP}^l E_N(600\text{ nm}) \approx 1.45 \times 10^{-4}\text{ nm}^{-1}$, $x_P^l \approx 0.75$, $E_N(600\text{ nm}) \approx 2.2 \times 10^{-3}\text{ nm}^{-1}$). This value is very unaccurate because it is determined from various parameters with experimental uncertainties.

The situation of DODCI in ethylene glycol is illustrated in fig. 16. For $\vartheta = 90°C$ the dash-dotted curve 4 gives $x_N^l E_N(\lambda)$. The remaining part (short-dashed curve) is practically equal to $x_P^l E_P(\lambda)$. A contribution $x_P^l \phi_{PN}^l E_N(\lambda)$ cannot be resolved.

This finding is in agreement with P-isomer accumulation studies [79] where a S_1-state P-isomer to S_0-state N-isomer transfer rate of ≈ 0.004 is determined. $q_P = \int E_P(\lambda)\, d\lambda$ of DODCI in ethylene glycol is plotted in fig. 18b.

(b) *Short-wavelength excitation.* The solid curves in fig. 13 (DODCI in methanol) and fig. 17 (DODCI in ethylene glycol) indicate only a small contribution of the P isomers to the fluorescence quantum distribution and the fluorescence quantum efficiency. The dashed curves in figs. 13 and 17 present $[x_P^l + \phi_{NP}^l(\lambda_L, \vartheta)] E_P(\lambda, \lambda_L, \vartheta)$ curves determined by the procedure described above in section 3.2.2.1. From the dashed curve in fig. 13a (DODCI in methanol, $\lambda_L = 590$ nm, $\vartheta = 60°C$) a value of $\phi_{NP}^l(590\text{ nm}, 60°C) \approx 0.065$ may be extracted ($(x_P^l + \phi_{NP}^l) E_P(635\text{ nm}) / E_{max} = 0.033$, $E_{max} = 2.18 \times 10^{-3}$ nm^{-1} (fig. 10), $E_P(635\text{ nm}) = 8.8 \times 10^{-4}$ (fig. 12), $x_P^l(590\text{ nm}, 60°C) \approx 0.0175$ (fig. 7)). The dashed curve in fig. 13b (DODCI in methanol, $\lambda_L = 510$ nm, $\vartheta = 0°C$) gives a value of $\phi_{NP}^l(510\text{ nm}, 0°C) \approx 0.078$. The extracted values from the dashed curves of fig. 17 (DODCI in ethylene glycol) are $\phi_{NP}^l(597\text{ nm}, 90°C) \approx 0.10$ and $\phi_{NP}^l(510\text{ nm}, 0°C) \approx 0.05$. The obtained ϕ_{NP}^l values are not very accurate because of the many experimental values that enter the determination. In ref. [79] a S_1-state N-isomer to S_0-state P-isomer transfer rate of $\approx 0.08 \pm 0.01$ has been determined for $\lambda_L = 514$ nm and $\vartheta = 25°C$.

In fig. 18, $q_N = [q - (x_P^l + \phi_{NP}^l) q_P] / x_N^l$ versus temperature is plotted. q_N is nearly equal to q since $(x_P^l + \phi_{NP}^l) q_P$ is only a small contribution and $x_N^l = 1 - x_P^l$ is nearly equal to 1.

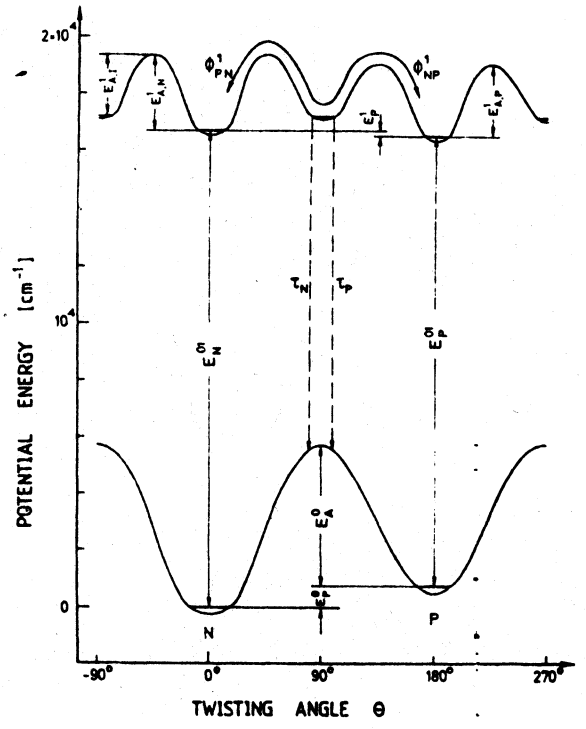

◀ Fig. 19. Potential energy model of DODCI versus twisting angle. Absolute scale belongs to DODCI in ethylene glycol. Depth $E^1_{A,I}$ of intermediate valley is undetermined.

3.3. Derivation of spectroscopic parameters

The absorption and fluorescence results are discussed by the S_0 double-valley and S_1 triple-valley potential energy surface diagram of fig. 19. The potential energy is plotted versus twisting angle. An out-of-plane twisting from a coiled form (N isomer) to an elongated form (P isomer) is assumed [13] (see inset on top of fig. 20, different coiled and elongated forms may exist). The spectroscopic analysis determines the zero-vibration S_0–S_1 energy gap of the N isomer, E^{01}_N and of the P isomer, E^{01}_P. Additionally the S_1-state barrier heights $E^1_{A,N}$ of the N isomer and $E^1_{A,P}$ of the *P* isomer are derived. No values for the intermediate S_1-state barrier $E^1_{A,I}$ are obtained. Only an upper value of $E^1_{A,I}$ may be estimated. The radiative S_1-state lifetimes $\tau_{rad,N}$ and $\tau_{rad,P}$ of the N isomer

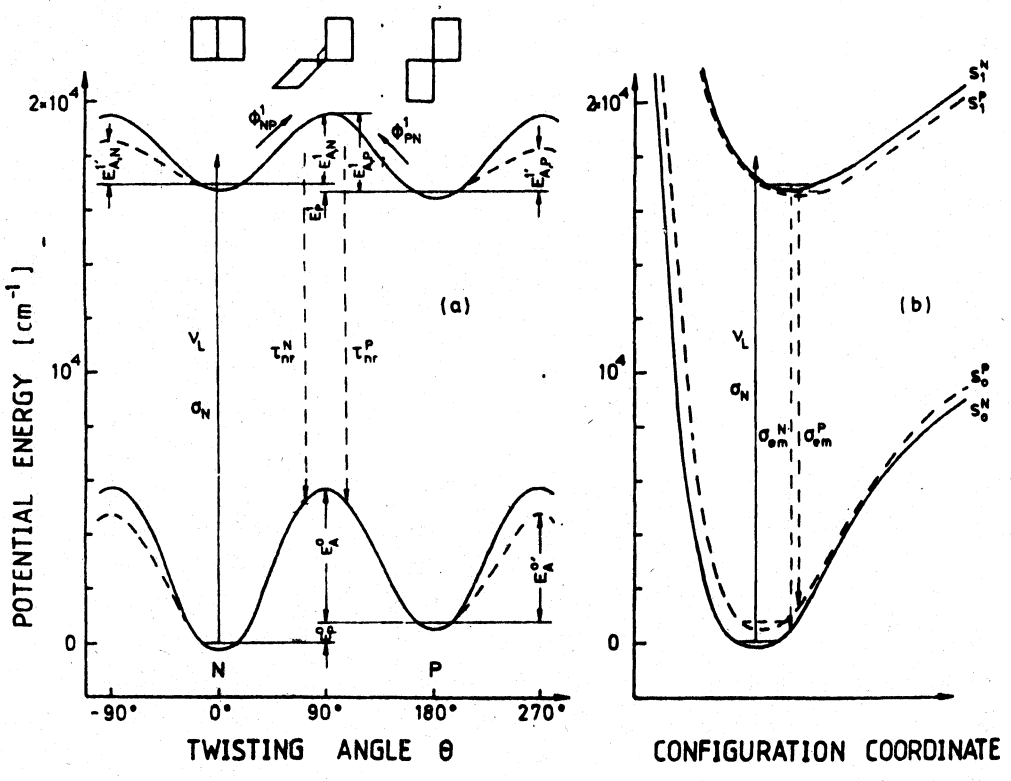

Fig. 20. (a) Limiting case of potential energy model of fig. 19. Absolute scale belongs to DODCI in methanol. Dashed potential energy curves are true potential energies without viscosity barrier contribution. (b) Potential energy versus vibrational configuration coordinate. Inset at top of (a) indicates schematically out-of-plane twisting.

and P isomer are calculated. The nonradiative S_1-state relaxation rates $k_{nr}^N = (\tau_{nr}^N)^{-1}$ and $k_{nr}^P = (\tau_{nr}^P)^{-1}$ of the N and P isomers are derived from the fluorescence quantum efficiencies.

In fig. 20a, a limiting form of fig. 19 is shown where the intermediate S_1-state barrier height diminishes ($E_{A,I}^1 = 0$, S_1-state potential energy curve reduces to a double-valley curve). Part (b) of fig. 20 shows the potential energy curves of the N and P isomers along a vibrational configuration coordinate. (N-isomer curves belong to twisting angle of $\theta = 0°$ and P-isomer curves belong to twisting angle of $\theta = 180°$.) The S_0–S_1 absorption follows the Franck–Condon transition principle. The excited vibrational states in the S_1-band thermalize quickly in relaxing to the S_1 potential minimum [85]. The excess heat energy is transferred quickly to the solvent [86].

The radiative lifetimes $\tau_{rad,N}$ and $\tau_{rad,P}$ of the N isomer and P isomer are derived from the absorption cross-section spectra (figs. 3–6) and the fluorescence quantum distribution spectra ($E_N(\lambda, \lambda_{0,N}, 22°C)$ and $E_P(\lambda, 22°C)$) by application of the Strickler–Berg formula [87,88] (i = N or P):

$$k_{rad,i} = \tau_{rad,i}^{-1} = \frac{8\pi n_{F,i}^3 c_0}{n_{A,i}} \frac{\int_{em} E_i(\lambda)\lambda \, d\lambda}{\int_{em} E_i(\lambda)\lambda^4 \, d\lambda} \int_{abs} \frac{\sigma_i(\lambda)}{\lambda} d\lambda . \quad (11)$$

$k_{rad,i}$ is the radiative transition rate. $n_{F,i}$ and $n_{A,i}$ are the average refractive indices of the solutions in the S_1–S_0 fluorescence region and the S_0–S_1 absorption region, respectively. The integrations extend over the S_1–S_0 emission (em) and the S_0–S_1 absorption regions (abs). The calculated radiative lifetimes are listed in table 1.

The stimulated emission cross-section spectra are derived from the fluorescence quantum distribution spectra by [89]

$$\sigma_{em,i}(\lambda) = \frac{\lambda^4 E_i(\lambda)}{8\pi n_F^2 c_0 \tau_{rad,i} \int_{em} E_i(\lambda) \, d\lambda} . \quad (12)$$

The stimulated emission cross-section spectra for the N isomers and the P isomers are included in figs. 3, 4 and 5, 6, respectively ($\vartheta = 22°C$).

The N-isomer and P-isomer S_1–S_0 fluorescence quantum efficiencies, q_N and q_P, are related to the radiative, nonradiative, and N–P S_1-state transfer rate constants $k_{rad,i}$, $k_{nr,i}$ and $k_{tr,ij}^1$ (i = N, P; j = P, N) by

$$q_i = \frac{k_{rad,i}}{k_{tot,i}} = \frac{k_{rad,i}}{k_{rad,i} + k_{nr,i} + k_{tr,ij}^1} = \left(1 + \frac{k_{nr,i}}{k_{rad,i}} + \frac{k_{tr,ij}^1}{k_{rad,i}}\right)^{-1} . \quad (13)$$

The N–P S_1-state transfer rate is

$$k_{tr,ij}^1 = \phi_{ij}^1 k_{tot,i} = \phi_{ij}^1 (k_{rad,i} + k_{nr,i} + k_{tr,ij}^1) = \frac{\phi_{ij}^1}{1-\phi_{ij}^1} (k_{rad,i} + k_{nr,i}) = \frac{\phi_{ij}^1}{1-\phi_{ij}^1} k_i = \frac{\phi_{ij}^1}{(1-\phi_{ij}^1)\tau_i} . \quad (14)$$

Insertion of eq. (14) into eq. (13) gives after some rearrangement

$$\frac{k_{nr,i}}{k_{rad,i}} = \frac{1-\phi_{ij}^1}{q_i} - 1 \approx \frac{1}{q_i} - 1 \quad (15)$$

and

$$\frac{k_{tr,ij}^1}{k_{rad,i}} = \frac{\phi_{ij}^1}{q_i} . \quad (16)$$

The approximation at the right-hand side of eq. (15) is valid for small ϕ_{ij}^1 values. Our experimental results give only rough values of ϕ_{PN}^1 and ϕ_{NP}^1 in the region between 0 and 10%. $k_{nr,i}$ is given generally by [90]

$$k_{nr,i} = \tau_{nr,i}^{-1} = k_{IC,i} + k_{TW,i} . \quad (17)$$

where $k_{IC,i}$ is the (temperature-independent) internal conversion rate constant (of a stiff molecule) and $k_{TW,i}$ is the twisting nonradiative decay constant. In our experiments the temperature-independent rate contribution seems to be negligibly small because $k_{nr,i}/k_{rad,i}$ becomes very small at low temperatures ($q \to 1$, fig. 9).

The normalized rate constants $k_{nr,N}/k_{rad,N}$ and $k_{nr,P}/k_{rad,P}$ versus inverse temperature are plotted in fig. 21a for DODCI in methanol and in fig. 21b for DODCI in ethylene glycol. They show an Arrhenius-type (Stern–Volmer-type) temperature dependence. For $k_{tr,NP}^1/k_{rad,N}$ and $k_{tr,PN}^1/k_{rad,P}$ no curves are presented because the ϕ_{NP}^1 and ϕ_{PN}^1 values are not very accurate.

The rotational deactivation rate constants $k_{m,i}$ (i = N,P) depend on the molecular solute–solvent friction ξ [5,91–94] and on the twisting barrier height. It is

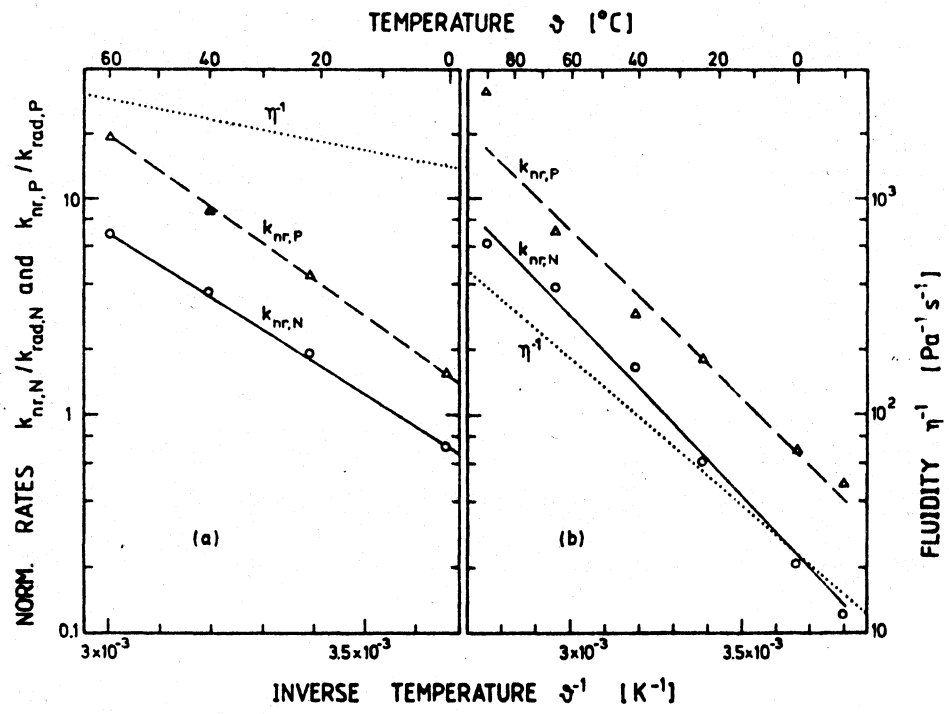

Fig. 21. Normalized relaxation rates of (a) DODCI in methanol and (b) DODCI in ethylene glycol. $k_{nr,N}/k_{rad,N}$ is represented by solid curves and experimental points (○) for $\lambda_L \approx \lambda_{0,N}$. $k_{nr,P}/k_{rad,P}$ is shown by dashed curves and experimental points (△). Dotted lines indicate the solvent fluidity (inverse viscosity) η^{-1}.

$$k_{nr,i} = \kappa(\xi) \exp(-E^{\ddagger}_{A,i}/k_B\vartheta) \approx (\kappa'/\xi) \exp(-E^{\ddagger}_{A,i}/k_B\vartheta) . \quad (18)$$

The temperature dependence of the molecular solute-solvent friction is also approximately given by an Arrhenius-type equation:

$$\xi^{-1} = \xi_0^{-1} \exp(-E_\xi/k_B\vartheta) . \quad (19)$$

Insertion of eq. (19) into eqs. (18) gives

$$k_{nr,i} \approx \kappa'' \exp\left(-\frac{E^{\ddagger}_{A,i}+E_\xi}{k_B\vartheta}\right) = \kappa'' \exp(-E^{\ddagger}_{A,i}/k_B\vartheta) . \quad (20)$$

The activation energies $E^{\ddagger}_{A,N}$ and $E^{\ddagger}_{A,P}$ are derived from the slopes of the curves of fig. 21 and are listed in table 1.

In the case of methanol the molecular solute-solvent friction ξ is approximately equal to the solvent viscosity η and E_ξ becomes equal to E_η [92]. For ethylene glycol the solute-solvent friction is less than the solvent viscosity [91,95]. The temperature dependences of η^{-1} (fluidity) [95] are included in figs. 21a and 21b and the E_η values are listed in table 1.

Since for methanol $E_\xi \approx E_\eta$, the intrinsic barrier heights $E^{\ddagger}_{A,i}$ of DODCI in methanol can be determined. The values are listed in table 1.

The potential energy curves of figs. 19 and 20 are drawn with quantitative energy values.

(i) The energy difference E^{01}_N between the relaxed S_1 state and the S_0 ground state of the N isomer is given by

$$E^{01}_N = h\nu_{0,N} = hc_0/\lambda_{0,N} ; \quad (21)$$

$\lambda_{0,N}$ is the wavelength where $\sigma_N = \sigma_{em,N}$ (figs. 3 and 4).

(ii) The zero-vibration energy difference, E^{01}_P, between the S_1 and S_0 state of the P isomer is determined by

$$E^{01}_P = h\nu_{0,P} = hc_0/\lambda_{0,P} . \quad (22)$$

At $\lambda_{0,P}$ it is $\sigma_P = \sigma_{em,P}$ (figs. 5 and 6).

(iii) The P-isomer ground-state level E_P^0 was determined previously by thermal population studies [30].

(iv) The ground-state P-isomer to N-isomer barrier height E_A^0 is taken from the literature [8] (DODCI in ethanol; the same values are assumed for the solvents methanol and ethylene glycol).

(v) The S_1-state energy level difference between the P isomer and the N isomer is given by

$$E_P^1 = E_N^{01} - E_P^0 - E_P^{01} . \tag{23}$$

(vi) The S_1-state intermediate barrier height $E_{A,I}^1$ remains undetermined. The presented fluorescence studies only give an approximate upper limit of $E_{A,I}^1 \lesssim E_{A,N}^1$, because for a considerably larger barrier height the S_1-state N- to P- and P- to N-isomer transfer would become negligibly small (no P-isomer fluorescence in case of N-isomer excitation and vice versa). The fluorescence spectra analysis seems to indicate a small S_1-state N- to P- and P- to N-transfer probability. A peak in the fluorescence spectra at the long-wavelength side ($\lambda > 730$ nm) due to fluorescence emission from the intermediate S_1-state valley would allow the determination of the barrier height $E_{A,I}^1$. Our fluorescence measurements were extended out to 1100 nm but no additional fluorescence peak could be observed:

$$\int_{730\text{ nm}}^{880\text{ nm}} E(\lambda)\,\mathrm{d}\lambda \approx 4\times 10^{-4} ,$$

$$\int_{880\text{ nm}}^{1100\text{ nm}} E(\lambda)\,\mathrm{d}\lambda < 10^{-4} .$$

The experimental results are compatible with $E_{A,I}^1 = 0$ (see fig. 20) since the necessary condition for this relation

$$E_N^{01} + E_{A,N}^1 = E_P^0 + E_P^{01} + E_{A,P}^1 , \tag{24}$$

or

$$\Delta E_{N,P}^1 = E_N^{01} + E_{A,N}^1 - E_P^0 - E_P^{01} - E_{A,P}^1 = 0 \tag{25}$$

is fulfilled within our experimental accuracy.

In the literature $E_{A,N}^1$ and E_A^0 are only found for DODCI in ethanol [8]. $E_{A,N}^1 = 1680 \pm 70\ \mathrm{cm}^{-1}$ [8] agrees reasonably well with our value of $E_{A,N}^1 = 2300 \pm 150\ \mathrm{cm}^{-1}$ for DODCI in methanol.

The P-isomer fluorescence quantum efficiencies are substantially smaller than the N-isomer fluorescence quantum efficiencies. This behaviour is thought to be due to the longer radiative lifetimes of the P isomers (table 1). For example the data at 22 °C are $q_N \approx 0.32$, $\tau_{F,N} = q_N \tau_{rad,N} \approx 0.8$ ns, $q_P \approx 0.18$, and $\tau_{F,P} \approx 0.9$ ns for DODCI in methanol. In the case of DODCI in ethylene glycol the data at 22 °C are $q_N \approx 0.60$, $\tau_{F,N} \approx 1.4$ ns, $q_P \approx 0.35$ and $\tau_{F,P} \approx 1.4$ ns. Time-resolved fluorescence lifetime measurements indicate comparable values of $\tau_{F,N}$ and $\tau_{F,P}$ [24]. Sometimes $\tau_{F,P}$ values shorter than $\tau_{F,N}$ values have been reported [2,12,21].

4. Conclusions

Absorption and fluorescence spectroscopic data of the mode-locking dye DODCI have been determined in the solvents methanol and ethylene glycol. The ethylene glycol results apply directly to the mode-locking situation in colliding pulse mode-locked or hybridly mode-locked dye lasers since DODCI in ethylene glycol is used in the dye jets. DODCI in acetonitile (an aprotic dipolar solvent) exhibits the same absorption spectrum and shows the same temperature dependence of the fluorescence spectra as DODCI in methanol.

The obtained spectroscopic data allow the drawing of a more quantitative potential energy curve versus twisting angle. In the S_1-state N-isomer and P-isomer barrier heights could be determined. The barrier height of the intermediate S_1-state valley remains still undetermined. Time-resolved fluorescence measurements [96,97], time-resolved excited-state absorption measurements [98,99] and time-resolved resonance CARS measurements [100,101] may help to clarify the situation.

An adiabatic photoisomerization of di-9-methylantracene in the S_1 state (chemical change takes place in the S_1 state) has been reported in ref. [102]. An "across-a-ridge-isomerization" of olefins in the triplet T_1 state is discussed in refs. [103–105]. The rotational isomerization of 2-vinylanthracene in the S_1 state has been proven recently by picosecond time-resolved fluorescence measurements using time-correlated single-photon counting techniques [97].

Acknowledgement

The authors thank Dr. I. Kügler and Mr. Endres of Osram, Munich, for providing the colour temperature data of the calibration lamp. They thank the Deutsche Forschungsgemeinschaft for financial support.

Appendix A. Fluorescence spectroscopic fundamentals

The fluorescence quantum distribution $E(\lambda)$ is defined by

$$E(\lambda)=S_1(\lambda)/P_A \tag{A.1}$$

and the fluorescence quantum efficiency is

$$q=\int_{em} E(\lambda)\,d\lambda\,. \tag{A.2}$$

$S_1(\lambda)$ is the intrinsic photon emission per wavelength interval (dimension photons per nm) and P_A is the number of absorbed photons of excitation light. P_A is given by

$$P_A=\frac{P_0(1-R_L)(1-T_L)}{1-R_L(1-T_L)}\,. \tag{A.3}$$

P_0 is the number of incident excitation photons to the fluorescing sample. The indices L stand for excitation light. $R_L=(n_L-1)^2/(n_L+1)^2$ is the reflectance of the excitation light at the entrance surface of the fluorescing sample. n_L is the refractive index at the excitation frequency ν_L. $T_L=\exp(-\sigma_L N_0 l)$ is the transmission of the excitation light through the sample. σ_L is the absorption cross section at the excitation frequency ν_L. N_0 is the number density of dye molecules, and l is the sample length. The term $R_L(1-T_L)$ in the denominator takes care of the back-reflected excitation light (geometric row).

The fluorescence quantum efficiency is measured relative to a reference dye of known fluorescence quantum efficiency q_R. It is

$$E(\lambda)=\frac{S_1(\lambda)}{\int_{em} S_{1,R}(\lambda)\,d\lambda}\frac{P_{A,R}}{P_A}=\frac{S_1(\lambda)}{\int S_{1,R}(\lambda)\,d\lambda}\frac{(1-R_{L,R})(1-T_{L,R})[1-R_L(1-T_L)]}{(1-R_L)(1-T_L)[1-R_{L,R}(1-T_{L,R})]}\,q_R\,. \tag{A.4}$$

when the number of incident excitation photons, P_0, is constant.

$S_1(\lambda)$ has to be related to $S_E(\lambda)$, the spectral fluorescence signal outside the fluorescence cell within a solid angle, $\Delta\Omega$, of signal detection. It is

$$S_E(\lambda)=S_1(\lambda)(1-R_F)(\Delta\Omega/4\pi n_F^2)f_{AE}(\lambda)\,. \tag{A.5}$$

$\Delta\Omega/n_F^2$ is the solid angle of detection inside the fluorescence cell. n_F is the average refractive index of the dye solution in the fluorescence spectral region. $R_F=(n_F-1)^2/(n_F+1)^2$ is the reflectance of the fluorescence light. $f_{AE}(\lambda)$ takes care of the multiple fluorescence re-absorption and re-emission. This factor is determined below.

Insertion of eq. (A.5) into eq. (A.4) gives

$$E(\lambda)=\frac{S_E(\lambda)f_{AE}(\lambda)}{\int S_{E,R}(\lambda)f_{AE,R}(\lambda)\,d\lambda}\frac{n_{F,R}^2}{n_F^2}\frac{1-R_F}{1-R_{F,R}}\frac{(1-R_{L,R})(1-T_{L,R})[1-R_L(1-T_L)]}{(1-R_L)(1-T_L)[1-R_{L,R}(1-T_{L,R})]}\,q_R\,. \tag{A.6}$$

The detected fluorescence signal $S_m(\lambda)$ (in photons per wavelength interval) is related to the spectral fluorescence signal, $S_E(\lambda)$ outside the sample by

$$S_m(\lambda)=S_E(\lambda)\mathrm{TF}(\lambda)\,. \tag{A.7}$$

The transfer function $\mathrm{TF}(\lambda)$ depends on the spectral characteristics of the polarizer, the spectrometer, and the

diode array detector (see fig. 2). The wavelength dependence of $TF(\lambda)$ is determined by measuring the spectral signal distribution $S_{m,lamp}(\lambda)$ of a halogen–tungsten lamp of known colour temperature ϑ_F [106,107]. It is

$$TF(\lambda)=\gamma S_{m,lamp}(\lambda)/\phi(\lambda,\vartheta_F)\,. \tag{A.8}$$

γ is a constant factor.

$$\phi(\lambda,\vartheta_F)=\frac{2\pi c_0}{\lambda^4[\exp(hc_0/k_B\lambda\vartheta_F)-1]} \tag{A.9}$$

is the Planck emission formula in photons/nm cm^2. For our calibrations a halogen–tungsten lamp of $\vartheta_F=3450\pm10$ K was used (Osram type HLX64625 halogen-projection bulb with 12 V voltage).

Insertion of eq. (A.7) into eq. (A.6) gives

$$E(\lambda)=\frac{S_m(\lambda)TF^{-1}(\lambda)f_{AE}(\lambda)}{\int S_m(\lambda)TF^{-1}(\lambda)f_{AE,R}(\lambda)\,d\lambda}\,\frac{n_{F,R}^2}{n_F^2}\,\frac{1-R_F}{1-R_{F,R}}\,\frac{(1-R_{L,R})(1-T_{L,R})[1-R_L(1-T_L)]}{(1-R_L)(1-T_L)[1-R_{L,R}(1-T_{L,R})]}\,q_R\,. \tag{A.10}$$

The multiple re-absorption and re-emission factor of the fluorescence light, $f_{AE}(\lambda)$, is determined in the following for the situation of front-face fluorescence detection [68]. Without re-absorption and re-emission of fluorescence light it is $f_{AE}(\lambda)=1$. The case of re-absorption of fluorescence light without re-emission is discussed in ref. [67]. The fluorescence reabsorption factor was found to be

$$f_A(\lambda)=\frac{\sigma_L}{\sigma_L+\sigma(\lambda)}\,\frac{1-T_L^{[\sigma_L+\sigma(\lambda)]/\sigma_L}}{1-T_L}\,. \tag{A.11}$$

$\sigma(\lambda)$ is the absorption cross section of the dye solution at wavelength λ. In the general case of multiple re-absorption and re-emission of fluorescence light it is

$$S_E(\lambda)=\sum_{i=0}^{\infty}S_E^{(i)}(\lambda)\,, \tag{A.12}$$

with

$$S_E^{(i+1)}(\lambda)\approx S_E^{(i)}(\lambda)[1-f_A(\lambda)]q \tag{A.13}$$

and

$$S_E^{(0)}(\lambda)=S_I(\lambda)(1-R_F)(\Delta\Omega/4\pi n_F^2)f_A(\lambda)\,. \tag{A.14}$$

Eq. (A.14) is equal to eq. (A.5) with $f_{AE}(\lambda)=f_A(\lambda)$ (no fluorescence emission of re-absorbed fluorescence light). The geometric row of eq. (A.12) gives

$$S_E(\lambda)=S_E^{(0)}(\lambda)/\{1-[1-f_A(\lambda)]q\} \tag{A.15}$$

and

$$f_{AE}(\lambda)=f_A(\lambda)/\{1-[1-f_A(\lambda)]q\}\,. \tag{A.16}$$

Insertion of eq. (A.16) into eq. (A.10) gives an implicit equation of the fluorescence quantum distribution, $E(\lambda)$ (q at right-hand side) which is solved numerically.

Appendix B. Light-induced accumulation of P isomers in S_0 ground state

The fluorescence spectrum of DODCI in methanol shows a clear P-isomer peak around 635 nm at a temperature of $\vartheta=-80$°C in the case of light excitation at $\lambda_L=590$ nm. This P-isomer fluorescence peak is thought to be due to light-induced accumulation of population in the S_0 ground state of the P isomer. At low temperature

the thermalization process between P and N isomers in the S_0 ground state becomes very slow. A small fraction of excited N-isomer molecules may relax to the P-isomer ground state. These molecules accumulate there and contribute to the P-isomer fluorescence by absorption of the excitation light.

The ground-state P-isomer to N-isomer transfer rate is [8,20,30]:

$$(\tau^0_{PN})^{-1} = k^0_{PN} = A_{iso} \exp(-E^0_A/k_B\vartheta) \tag{B.1}$$

and the N-isomer to P-isomer transfer rate is

$$(\tau^0_{NP})^{-1} = k^0_{NP} = A_{iso} \exp[-(E^0_A + E^0_P)/k_B\vartheta] . \tag{B.2}$$

The pre-exponential factor A_{iso} and the ground-state activation energy E^0_A have been determined in ref. [8] for DODCI in ethanol. The values are $A_{iso} \approx 1.9\times10^{13}\ s^{-1}$ and $E^0_A \approx 9.95\times10^{-20}$ J. E^0_P is listed in table 1. A_{iso} and E^0_A are thought to be approximately the same for methanol and ethylene glycol as is confirmed by the similar relaxation times τ^0_{PN} at room temperature measured for ethanol, methanol and ethylene glycol [20]. In fig. 22, τ^0_{PN} and τ^0_{NP} are plotted versus temperature ϑ ($E^0_P = 703\ cm^{-1}$ is used). At $\vartheta = -80$°C, values of $\tau^0_{PN} \approx 850$ s and $\tau^0_{NP} \approx 1.6\times10^5$ s are calculated.

The ground-state P-isomer population will accumulate if the population rate from the S_1 state is larger than the depopulation rate k^0_{PN}. The population rate depends on the excitation light intensity I_L. Appreciable accumulation of population occurs if I_L is larger than the saturation intensity of accumulation, $I^0_{S,P}$, which is defined

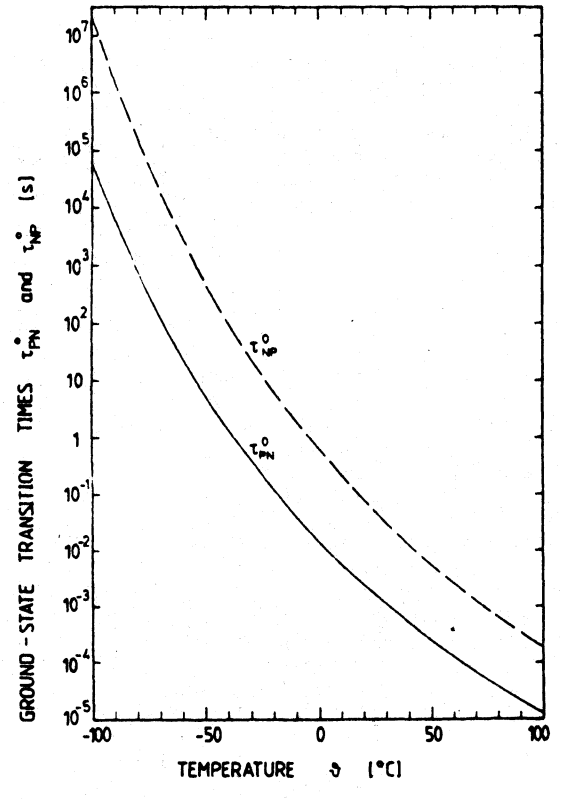

Fig. 22. Ground-state P- to N-isomer relaxation time τ^0_{PN} and N- to P-isomer transition time τ^0_{NP} versus temperature. The curves belong to eqs. (B.1) and (B.2) with $A_{iso} = 1.9\times10^{13}\ s^{-1}$, $E^0_A = 9.95\times10^{-20}$ J, and $E^0_P = 1.4\times10^{-20}$ J [8,30].

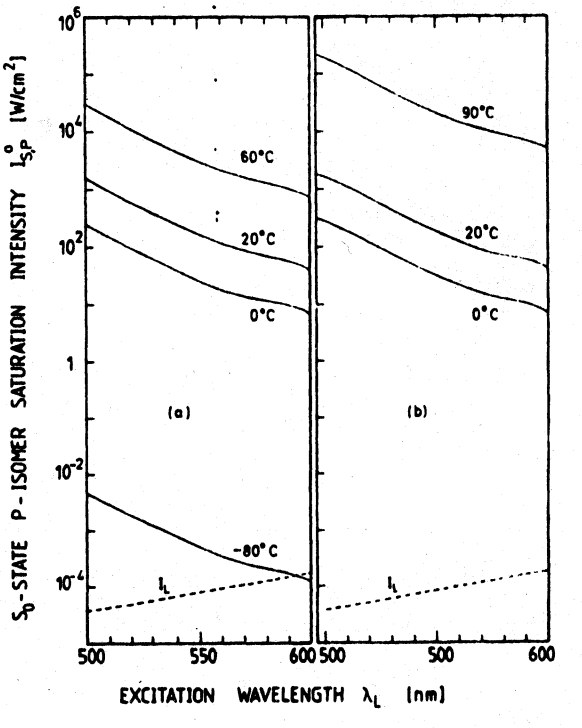

Fig. 23. Ground-state P-isomer saturation intensities of accumulation, $I^0_{S,P}$, versus excitation wavelength, λ_L, for various temperatures. The short-dashed curve represents roughly the experimental intensity of excitation light in the sample. (a) DODCI in methanol. (b) DODCI in ethylene glycol.

by $N_{P,0}/N_{N,0}=x_P^0(I_L=\infty)/2$. In the case of dominant S_1-state N–P transfer ($\phi_{NP}^1>\phi_{NP}^{10}$, $\phi_{PN}^1>\phi_{PN}^{10}$), $I_{S,P}^0$ is given by [79]

$$I_{S,P}^0=\frac{h\nu_L(1-\phi_{NP}^1\phi_{PN}^1)[1-\exp(-E_P^0/k_B\vartheta)]}{\sigma_P(\lambda_L)\tau_{PN}^0\phi_{PN}^1[1-\phi_{NP}^1+2(1-\phi_{PN}^1)\phi_{NP}^1\sigma_N(\lambda_L)/\phi_{PN}^1\sigma_P(\lambda_L)]}\approx\frac{h\nu_L}{\sigma_P(\lambda_L)\tau_{PN}^0\phi_{PN}^1}. \quad (B.3)$$

In the case of dominant direct S_1-state to S_0-state N-isomer to P-isomer and P-isomer to N-isomer transfer [8] with transfer rates ϕ_{NP}^{10} and ϕ_{PN}^{10}, eq. (B.3) remains valid in the case of $\phi_{NP}^{10}\ll 1$ and $\phi_{PN}^{10}\ll 1$ if ϕ_{NP}^1 and ϕ_{PN}^1 are replaced by ϕ_{NP}^{10} and ϕ_{PN}^{10}, respectively.

In fig. 23, $I_{S,P}^0$ of DODCI in methanol (a) and ethylene glycol (b) is plotted versus excitation wavelength λ_L for various temperatures. $\phi_{PN}^1=0.01$ (equivalent to $\phi_{PN}^{10}=0.01$) is used for the calculation of the curves. The applied excitation intensity I_L is included in fig. 23. For DODCI in methanol at $\vartheta=-80$ °C and $\lambda_L=590$ nm it is $I_L\approx I_{S,P}^0$. For this case enhanced P-isomer fluorescence has been observed experimentally (curve 1 of fig. 10). For all the other experimental situations it is $I_L\ll I_{S,P}^0$ and P-isomer accumulation in the S_0 state plays no role. Even for DODCI in methanol at $\vartheta=-80$ °C and $\lambda_L=510$ nm is I_L already small compared to $I_{S,P}^0$.

References

[1] D.N. Dempster, T. Morrow, R. Rankin and G.F. Thompson, J. Chem. Soc. Faraday Trans. II (1972) 1479.
[2] E.G. Arthurs, D.J. Bradley and A.G. Roddie, Chem. Phys. Letters 22 (1973) 230.
[3] E.G. Arthurs, D.J. Bradley and A.G. Roddie, Opt. Commun. 8 (1973) 118.
[4] S.P. Velsko and G.R. Fleming, Chem. Phys. 65 (1982) 59.
[5] S.P. Velsko, D.H. Waldeck and G.R. Fleming, J. Chem. Phys. 78 (1983) 249.
[6] K. Kasatani, M. Kawasaki and H. Sato, J. Phys. Chem. 88 (1984) 5451.
[7] G.M. Bilmes, J.O. Tocho and S.E. Braslavsky, Chem. Phys. Letters 134 (1987) 335.
[8] C. Rulliere, Chem. Phys. Letters 43 (1976) 303.
[9] C. Rulliere and J. Joussot-Dubien, Compt. Rend. Acad. Sci. (Paris) 283, Ser. C (1976) 249.
[10] X.R. Zhu and J.M. Harris, Chem. Phys. 124 (1988) 321.
[11] D.J. Bradley, in: Topics in Applied Physics, Vol. 18. Ultrashort Light Pulses, ed. L.S. Shapiro (Springer, Berlin, 1977) pp. 17 ff.
[12] J.C. Mialocq, A.W. Boyd, J. Jaraudias and J. Sutton, Chem. Phys. Letters 37 (1976) 236.
[13] G.R. Fleming, A.E.W. Knight, J.M. Morris, R.J. Robbins and G.W. Robinson, Chem. Phys. Letters 49 (1977) 1.
[14] D. Madge and M.W. Windsor, Chem. Phys. Letters 27 (1974) 31.
[15] G.E. Busch, K.S. Greve, G.L. Olson, R.P. Jones and P.M. Rentzepis, Chem. Phys. Letters 33 (1975) 412.
[16] G.E. Busch, K.S. Greve, G.L. Olson, R.P. Jones and P.M. Rentzepis, Chem. Phys. Letters 33 (1975) 417.
[17] D. Doizi and J.C. Mialocq, Compt. Rend. Acad. Sci. (Paris) 297, Ser. II (1983) 109.
[18] J.C. Mialocq, D. Doizi and M.P. Gingold, Chem. Phys. Letters 103 (1983) 225.
[19] J. Jaraudias, P. Goujon and J.C Mialocq, Chem. Phys. Letters 45 (1977) 107.
[20] J. Jaraudias, J. Photochem. 13 (1980) 35.
[21] D. Khetchinashwili, S. Rentsch, B. Schröder and H. Wabnitz, in: Proceedings of the 4th International Symposium on Ultrafast Phenomena in Spectroscopy, Reinhardtsbrunn, October 1985, Teubner Texte zur Physik, Vol. 10 (Teubner, Leipzig, 1985) p. 234.
[22] E.V. Sitzmann and K.B. Eisenthal, J. Phys. Chem. 92 (1988) 4579.
[23] C.V. Shank and E.P. Ippen, Appl. Phys. Letters 26 (1975) 62.
[24] F. Heisel, J.A. Miehé and B. Sipp, J. Luminescence 24/25 (1981) 651.
[25] D.H. Waldeck and G.R. Fleming, J. Phys. Chem. 85 (1981) 2614.
[26] S. Schneider, U. Möller and H. Coufal, Appl. Opt. 21 (1982) 44.
[27] S. Rentsch, F. Döpel and V. Petrov, Appl. Phys. B 46 (1988) 357.
[28] L. Scaffardi, G.M. Bilmes, D. Schinca and J.O. Tocho, Chem. Phys. Letters 140 (1987) 163.
[29] G.M. Bilmes, J.O. Tocho and S.E. Braslavsky, J. Phys. Chem. 92 (1988) 5958.
[30] W. Bäumler and A. Penzkofer, Chem. Phys. Letters 150 (1988) 315.
[31] S. Rentsch, U.W. Grummt and D. Khetchinashwili, Laser Chem. 7 (1987) 261.
[32] E.N. Kaliteevskaya, T.K. Razumova and E.P. Shchelkina, Opt. Spectry. 60 (1986) 51.
[33] E.N. Kaliteevskaya, T.K. Razumova and G.M. Rubanova, Opt. Spectry. 60 (1986) 166.
[34] F. Momicchioli, I. Baraldi and G. Berthier, Chem. Phys. 123 (1988) 103.
[35] G. Orlandi and W. Siebrand, Chem. Phys. Letters 30 (1975) 352.
[36] A.P. Darmanyan, V.A. Kuzmin and Yu.E. Borisevich, Izv. Akad. Nauk SSSR Ser. Khim. No. 2 (1979) 349.
[37] S.K. Rentsch, Chem. Phys. 69 (1982) 81.
[38] W. Schmidt and F.P. Schäfer, Phys. Letters A 26 (1968) 558.

[39] D.J. Bradley, A.J.F. Durrant, F. O'Neill and B. Sutherland, Phys. Letters A 30 (1969) 535.
[40] D.J. Bradley and F. O'Neill, Opto-Electron. 1 (1969) 69.
[41] D.J. Bradley, B. Liddy, A.G. Roddie, W. Sibbett and W. Sleat, Opt. Commun. 3 (1971) 426.
[42] P.R. Bird, D.J. Bradley and W. Sibbett, in: Proceedings of the 11th International Congress on High Speed Photography (Chapman and Hall, London, 1975) p. 112.
[43] E.P. Ippen, C.V. Shank and A. Dienes, Appl. Phys. Letters 21 (1972) 348.
[44] C.V. Shank and E.P. Ippen, in: Topics in Applied Physics, Vol. 18. Ultrashort Laser Pulses, ed. S.L. Shapiro (Springer, Berlin, 1977) p. 121.
[45] C.V. Shank, in: Topics in Applied Physics, Vol. 1. Dye Lasers, ed. F.P. Schäfer, 2nd revised Ed. (Springer, Berlin, 1977) pp. 5 ff.
[46] C.V. Shank, in: Topics in Applied Physics, Vol. 60. Ultrashort Laser Pulses and Applications, ed. W. Kaiser (Springer, Berlin, 1988) pp. 5 ff.
[47] C.V. Shank and E.P. Ippen, Appl. Phys. Letters 24 (1974) 373.
[48] S. Schneider, Phil. Trans. Roy. Soc. A 298 (1980) 233.
[49] Y. Ishida, T. Yajima and K. Naganuma, Japan. J. Appl. Phys. 19 (1980) L717.
[50] R.L. Fork, B.I. Greene and C.V. Shank, Appl. Phys. Letters 38 (1981) 671.
[51] R.L. Fork, O.E. Martinez and J.P. Gordon, Appl. Phys. Letters 9 (1984) 150.
[52] J.A. Valdmanis, R.L. Fork and J.P. Gordon, Opt. Letters 10 (1985) 131.
[53] J.J. Fontaine, W. Dietel and J.C. Diels, IEEE J. Quantum Electron. QE-19 (1983) 1467.
[54] J.C. Diels, W. Dietel, J.J. Fontaine, W. Rudolph and B. Wilhelmi, J. Opt. Soc. Am. B 2 (1985) 680.
[55] J. Chesnoy and L. Fini, Opt. Letters 11 (1986) 635.
[56] J.A. Valdmanis and R.L. Fork, IEEE J. Quantum Electron. QE-22 (1986) 112.
[57] O.E. Martinez, R.L. Fork and J.P. Gordon, J. Opt. Soc. Am. B 2 (1985) 753.
[58] A. Penzkofer, Appl. Phys. B 46 (1988) 43.
[59] V. Petrov, W. Rudolph, U. Stamm and B. Wilhelmi, Technical Digest of IQEC'88, July 18–21, 1988, Tokyo, Japan, p. Tu-A4.
[60] V. Petrov, W. Rudolph and B. Wilhelmi, Rev. Phys. Appl. 22 (1987) 1639.
[61] F.P. Schäfer, W. Schmidt and K. Marth, Phys. Letters A 24 (1967) 280.
[62] M. Maeda and Y. Miyazoe, Japan. J. Appl. Phys. 11 (1972) 692.
[63] F.B. Dunning and E.D. Stokes, Opt. Commun. 6 (1972) 160.
[64] P.K. Runge, Opt. Commun. 5 (1972) 311.
[65] A. Hirth and K. Vollrath, Opt. Commun. 7 (1973) 339.
[66] V. Petrov and C. Rempel, Chem. Phys. Letters 148 (1988) 26.
[67] A. Penzkofer and W. Leupacher, J. Luminescence 37 (1987) 61.
[68] K.A. Selanger, J. Falnes and T. Sikkeland, J. Phys. Chem. 81 (1977) 1960.
[69] A. Bączyński, T. Marszalek, H. Walerys and B. Zietek, Acta Phys. Polon. 44 (1973) 805.
[70] J.S. Batchelder, A.H. Zewail and T. Cole, Appl. Opt. 20 (1981) 3733.
[71] R. Sens, Dissertation, Universität-Gesamthochschule Siegen, Siegen (1984).
[72] K.H. Drexhage, Laser Focus 9, No. 3 (1973) 35.
[73] T. Karstens and K. Kobs, J. Chem. Phys. 84 (1980) 1871.
[74] R.F. Kubin and A.N. Fletcher, J. Luminescence 27 (1982) 455.
[75] D. Madge, J.H. Brannon, T.L. Cremers and J. Ohmsted III, J. Chem. Phys. 83 (1979) 696.
[76] D.F. Eaton, EPA Newsletter 28 (1986) 21.
[77] R. Sens and K.H. Drexhage, J. Luminescence 24/25 (1981) 709.
[78] W. Blau, W. Dankesreiter and A. Penzkofer, Chem. Phys. 85 (1984) 473.
[79] W. Bäumler and A. Penzkofer, to be published.
[80] K. Rotkiewicz, K.H. Grellmann and Z.R. Grabowski, Chem. Phys. Letters 19 (1973) 315.
[81] Z.R. Grabowski and J. Dobkowski, Pure Appl. Chem. 55 (1983) 245.
[82] W. Rettig, Angew. Chem. Intern. Ed. 25 (1986) 971.
[83] W. Rettig, Appl. Phys. B 45 (1988) 145.
[84] S.G. Su and J.D. Simon, J. Chem. Phys. 89 (1988) 908.
[85] G. Angel, R. Gagel and A. Laubereau, Chem. Phys. 131 (1989) 129.
[86] A. Seilmeier and W. Kaiser, in: Topics in Applied Physics, Vol. 60. Ultrafast Laser Pulses and Applications, ed. W. Kaiser (Springer, Berlin, 1988) pp. 279 ff.
[87] S.J. Strickler and R.A. Berg, J. Chem. Phys. 37 (1962) 814.
[88] J.B. Birks and D.J. Dyson, Proc. Roy. Soc. A 275 (1963) 135.
[89] O.G. Peterson, J.P. Webb, W.C. McColgin and J.H. Eberly, J. Appl. Phys. 42 (1971) 1917.
[90] M. Vogel, Dissertation, Technische Universität Berlin, Berlin (1987).
[91] G.R. Fleming, Chemical Applications of Ultrafast Spectroscopy (Oxford Univ. Press, London, 1986).
[92] J.M. Hicks, M.T. Vandersall, E.V. Sitzmann and K.B. Eisenthal, Chem. Phys. Letters 135 (1987) 413.
[93] N.S. Park, N. Sivakumar, E.A. Hoburg and D.H. Waldeck, in: Springer Series in Chemical Physics, Vol. 58. Ultrafast Phenomena VI, eds. T. Yajima, K. Yoshihara, C.B. Harris and S. Shionoya (Springer, Berlin, 1988) p. 551.
[94] T.J. Chuang and K.B. Eisenthal, Chem. Phys. Letters 11 (1971) 368.
[95] R.C. Weast, ed., CRC Handbook of Chemistry and Physics, 1st Student Edition (CRC Press, Boca Raton, 1988) p. F-21.
[96] A.M. Brearley, S.R. Flom, V. Nagarajan and P.F. Barbara, J. Phys. Chem. 90 (1986) 2092.
[97] T. Arai, T. Karatsu, H. Sakuragi, K. Tokumaru, N. Tamai and I. Yamazaki, Chem. Phys. Letters 158 (1989) 429.

[98] W. Zinth, J. Dobler, K. Dressler and W. Kaiser, in: Springer Series in Chemical Physics, Vol. 48. Ultrafast Phenomena VI, eds. T. Yajima, K. Yoshihara, C.B. Harris and S. Shionaya (Springer, Berlin, 1988) p. 581.
[99] N.P. Ernsting, in: Proceedings of the 6th International Symposium on Ultrafast Phenomena in Spectroscopy, Aug. 23–27, 1989, Neubrandenburg, GDR, eds. E. Klose and B. Wilhelmi, Springer Series in Chemical Physics (Springer, Berlin, 1989), to be published.
[100] W. Werncke, A. Lau, M. Pfeiffer, H.-J. Weigmann, W. Freyer, T.J. Tscholl and K.M. Bok, Chem. Phys. 118 (1987) 113.
[101] A. Lau, W. Werncke, M. Pfeiffer, H.-J. Weigmann and K.M. Bok, J. Raman Spectry. 19 (1988) 517.
[102] J. Menter and Th. Förster, Photochem. Photobiol. 15 (1972) 289.
[103] H. Misawa, T. Karatsu, T. Arai, H. Sakuragi and K. Tokumaru, Chem. Phys. Letters 146 (1988) 405.
[104] T. Arai, T. Karatsu, M. Tsuchiya, H. Sakuragi and K. Tokumaru, Chem. Phys. Letters 149 (1988) 161.
[105] T. Arai, H. Okamoto, H. Sakuragi and K. Tokumaru, Chem. Phys. Letters 157 (1989) 46.
[106] H. Hoppmann and K.E. Wuttke, Tech. Wiss. Abh. Osram Ges. 9 (1967) 137.
[107] G.M. Neumann, Lichttechnik 21 (1969) 63A.